



AGU Advances

Original Version of

Column-Compound Extremes in the Global Ocean

Joel Wong¹, Matthias Münnich¹, and Nicolas Gruber¹

¹Environmental Physics, Institute of Biogeochemistry and Pollutant Dynamics, ETH Zurich, Zurich, Switzerland

Column-Compound Extremes in the Global Ocean

Joel Wong¹, Matthias Münnich¹, and Nicolas Gruber¹

¹Environmental Physics, Institute of Biogeochemistry and Pollutant Dynamics, ETH Zurich, Zürich, Switzerland

Key Points:

- Column-compound extremes (CCX): defined when 50 m of the top 300 m is extreme in multiple parameters, reduce habitable space by up to 75%.
- From 1961 to 2020, CCX have become more intense, longer, and occupy more volume, driven by the trends in ocean warming and acidification.
- Triple CCX are largely confined to the tropics and the North Pacific, have high intensity, and severely reduces habitable space.

Corresponding author: Joel Wong, joel.wong@usys.ethz.ch

Abstract

Marine extreme events such as marine heatwaves, ocean acidity extremes and low oxygen extremes can pose a substantial threat to marine organisms and ecosystems. Such extremes might be particularly detrimental (i) when they occur compounded in more than one stressor, and (ii) when the extremes extend substantially across the water column, restricting the habitable space for marine organisms. Here, we use daily output of a hindcast simulation (1961-2020) from the ocean component of the Community Earth System Model to characterise such column-compound extreme events (CCX), employing a relative threshold approach to identify extremes and requiring them to extend vertically over at least 50 m. The diagnosed CCXs are prevalent, occupying worldwide in the 1960s about 1% of the volume contained within the top 300 m. Over the duration of our simulation, CCXs become more intense, last longer, and occupy more volume, driven by the trends in ocean warming and ocean acidification. For example, the triple CCX expanded 24-fold, now last 3-times longer, and became 6-times more intense since the early 1960s. Removing this effect with a moving baseline permits us to better understand the key characteristics of the CCXs. They last typically about 10 to 30 days and predominantly occur in the tropics and the high latitudes, regions of high potential biological vulnerability. Overall, the CCXs fall into 16 clusters, reflecting different patterns and drivers. Triple CCX are largely confined to the tropics and the North Pacific, and tend to be associated with the El Niño-Southern Oscillation.

Plain Language Summary

The global ocean is getting warmer, more acidic, and losing oxygen due to climate change. On top of this trend, sudden increases in temperature, or drops in pH or oxygen adversely affect marine organisms when they cannot quickly adapt to these extreme conditions. These conditions are worse for marine organisms when such extremes occur together in the vertical water column leading to a column-compound extreme (CCX) event, severely reducing the available habitable space. To investigate such CCXs, we use a numerical model simulation of the global ocean during the historical period of 1961 to 2020. Singular extreme events are identified primarily with relative percentile thresholds, while CCXs require a 50 m minimum depth threshold in the water column. We find that CCXs have been increasing in volume, occupying up to 20% of the global ocean volume towards 2020. We then remove the climate trend to better understand the drivers behind CCXs. Many CCXs occur in the tropics and high latitudes, lasting 10 to 30 days and reducing habitable space by up to 75%. This study is the first to systematically detect compound extremes in the water column, and forms the basis to determine their detrimental effects on marine organisms and ecosystems.

1 Introduction

Climate change has measurably warmed the ocean, increased its acidity, and decreased its oxygen content (Masson-Delmotte et al., 2021). These trends are punctuated by extreme events whose intensities and rapid onsets possibly impact marine organisms and ecosystems more than the slowly evolving trends do (Collins et al., 2019; Gruber et al., 2021). The study of marine extremes emerged forcefully in the last decade, with the vast majority of studies having focused on marine heatwaves (Hobday et al., 2016; Holbrook, Sen Gupta, et al., 2020; Oliver et al., 2021), their drivers (Holbrook et al., 2019; Sen Gupta et al., 2020), and impacts (Smale et al., 2019; K. E. Smith et al., 2023). But also ocean acidity extremes (OAX) (Hauri et al., 2013; Kwiatkowski & Orr, 2018; Negrete-García et al., 2019; Burger et al., 2020; Desmet et al., 2022) and low oxygen extremes (LOX) (Chan et al., 2008; Hofmann et al., 2011; Leung, Mislán, et al., 2019; Köhn et al., 2022) are receiving increasing attention, with the study of compound marine extremes, that is, events when conditions are extreme in more than one stressor emerging as an

62 issue of special concern(Gruber et al., 2021; Le Grix et al., 2021; Burger et al., 2022; Le Grix
63 et al., 2022).

64 Such compounded extreme events can have a disproportionately large impact on
65 marine biota, especially when the different stressors act synergistically, that is, when they
66 reinforce each other (Crain et al., 2008; Boyd & Brown, 2015; Pirota et al., 2022). A
67 well-known example is the decrease of aerobic metabolic rates with increasing temper-
68 ature and decreasing oxygen (Pörtner & Knust, 2007; Deutsch et al., 2015), making ec-
69 totherms especially susceptible to compounded MHW and LOX. Bednaršek et al. (2018)
70 also showed biological implications for pteropods during anomalously high temperature
71 and acidity events (the latter corresponding to anomalously low pH events, with $\text{pH} =$
72 $-\log[\text{H}^+]$, and $[\text{H}^+]$ being the concentration of the hydrogen ion). Extremes can be com-
73 pounded in different ways that lead to amplified impacts on organisms and ecosystems.
74 Multiple extremes occurring at the same time and place has been explored with prop-
75 erties such as temperature and pH (Burger et al., 2022), temperature and chlorophyll
76 (Le Grix et al., 2021), pH and oxygen (Nam et al., 2011; Köhn et al., 2022), and for triple
77 extremes involving pH, oxygen, and temperature (Gruber et al., 2021).

78 Warming of the ocean over the past 150 years and the strong trend in ocean acid-
79 ification have lead to a substantial increases in the MHW and OAX extremes associated
80 with these stressors (Oliver et al., 2018; Gruber et al., 2021) and are bound to increase
81 in the future as long these driving trends continue (Frölicher et al., 2018). For example,
82 Oliver et al. (2018) showed that between 1925 to 2016, the frequency and duration of
83 MHW increased by 34% and 17%, respectively, resulting globally in a more than 50%
84 increase in the number of MHW days. For OAX, the trends are even stronger, going from
85 a pre-industrial situation with about 4 days with extreme conditions to a nearly perma-
86 nent state of extremes (Gruber et al., 2021; Burger et al., 2022). Corresponding trends
87 are also expected for the LOX extremes driven by ocean deoxygenation (Gruber et al.,
88 2021), but the global ocean deoxygenation trends tend to be smaller compared to the
89 level of variability, leading to smaller, and not yet well established trends in LOX. As
90 a consequence of these trends in the single stressor extremes, compound extremes must
91 increase as well. Gruber et al. (2021) attributed, for example, the development of wide-
92 spread double compound extremes in the Northeast Pacific over the past 40 years, and
93 especially the triple-compound extreme at the height of the "Blob" event, in part, to the
94 underlying trends ocean warming, acidification, and deoxygenation. They speculated,
95 that part of the broad ecological impacts of the "Blob" might be caused by these com-
96 pound extremes. However, in order to understand the mechanisms driving the extremes,
97 it is better to remove the trend in the extremes, by using a so-called moving baseline (Oliver
98 et al., 2021; Burger et al., 2020; Gruber et al., 2021; Burger et al., 2022). Analysis of ex-
99 tremes, and especially compound extremes on a moving baseline is also appropriate when
100 considering the impact of these extremes on organisms that have the capacity to adapt
101 to the more slowly evolving changes in temperature, ocean acidification, and oxygen (see
102 also discussion by Sen Gupta (2023)).

103 So far, the vast majority of MHW studies have focused on the surface ocean only,
104 disregarding the fact that many organisms might have the potential to migrate to colder
105 temperatures at deeper depths when a surface heat wave affects them (Jorda et al., 2020).
106 Furthermore, the habitat of vertically migrating organisms can be considered to include
107 the water column down to about 400 m (Bianchi et al., 2013; Bianchi & Mislán, 2016).
108 Detecting extremes across the vertical dimension is thus an important step towards un-
109 derstanding the compression of habitable space during such extremes. Some MHW stud-
110 ies have looked into the subsurface, (Schaeffer & Roughan, 2017; Elzahaby et al., 2021;
111 Scannell et al., 2020; McAdam et al., 2022; Fragkopoulou et al., 2023), while the con-
112 cept of habitat compression has been considered with respect to temperature and oxy-
113 gen changes (Jorda et al., 2020; Köhn et al., 2022). However, a consistent definition of
114 compound extremes in the column has yet to be defined. The well-studied surface MHW

115 may extend into subsurface, compounding vertically with OAX and LOX to deteriorate
116 the habitable conditions of the water column.

117 Marine extremes can be driven by various mechanisms, and the study of compounded
118 extremes in the vertical dimension increases the complexity of this task (Gruber et al.,
119 2021). Surface MHWs are understood to be primarily driven either from the atmosphere
120 through anomalous air-sea heat fluxes, or by lateral heat advection (Sen Gupta et al.,
121 2020; Holbrook, Sen Gupta, et al., 2020; Marin et al., 2022). Such surface MHWs may
122 cause higher stratification in the upper ocean, suppressing the upwelling of carbon-rich
123 and low-oxygen waters and hence, decreasing the likelihood of surface OAX and LOX.
124 However, temperature anomalies have been shown to influence OAX occurrence by shift-
125 ing the carbonate chemistry equilibrium or modulating dissolved organic carbon (DIC)
126 (Burger et al., 2022), thereby increasing or decreasing $[H^+]$ respectively. At depth, ver-
127 tical or lateral displacement of waters across strong gradients in temperature, $[H^+]$, or
128 oxygen tends to be an important driver of extremes there, with the orientation of the
129 gradients being key for determining the nature of the compounded extreme. But there
130 are many other mechanisms, involving also biological physical interactions, e.g., in mesoscale
131 eddies (Gruber et al., 2021; Köhn et al., 2022; Desmet et al., 2022) that are key for gen-
132 erating and maintaining marine extremes at depth. Considering the various physical, chem-
133 ical, and biogeochemical processes in the ocean, inferring the mechanisms behind com-
134 pound extreme events can be a complex task. Extremes which are compounded may share
135 a common driver, be driven by one another, or co-occur in the column with different drivers
136 (Gruber et al., 2021). With percentile thresholds, some detected compound extremes may
137 arise purely out of statistical chance (Burger et al., 2022). Extremes with affiliated drivers
138 have a higher propensity of co-occurrence above such a random signal. Such compound
139 extremes are significant and merit investigation.

140 Extreme events across the globe have been linked to large scale climate modes, the
141 dominant one being the El Niño-Southern Oscillation (ENSO) (Santoso et al., 2017; Hol-
142 brook, Claar, et al., 2020). The prevalence of ENSO in the study of marine extremes is
143 partly due to the large area it affects in the Pacific, but also due to its teleconnections
144 with other ocean basins (Roy & Reason, 2001; Luo et al., 2010). ENSO events are trig-
145 gered by changes in the winds in the eastern tropical Pacific, but they affect, through
146 connected changes in large-scale ocean and atmospheric circulations, many remote re-
147 gions (aka teleconnections). While ENSO might not directly cause the extreme, the ENSO-
148 driven changes in the mean state can make the occurrence of extremes more likely or pro-
149 long and intensify existing extremes. A good example is the 2013-2015 "Blob" marine
150 heatwave in the Northeast Pacific, which turned into one of the world's largest and longest
151 lasting MHW owing to the coalescence of regional circulation changes and ENSO-driven
152 warming (Di Lorenzo & Mantua, 2016; Holbrook et al., 2019; Gruber et al., 2021). ENSO
153 has also been linked to MHWs in the Indian and Southern oceans (Holbrook et al., 2019;
154 Sen Gupta et al., 2020; Oliver et al., 2021). In addition, ENSO has been shown to strongly
155 affect also OAX and LOX in the Pacific ocean, especially at depth (Turi et al., 2018; Le-
156 ung, Thompson, et al., 2019; Köhn et al., 2022; Desmet et al., 2023).

157 Here, we extend the existing work on marine extremes by expanding our analysis
158 simultaneously in two directions. We expand in depth by analyzing extremes across the
159 whole upper water column, and we expand in terms of stressors by focusing on compound
160 events. Thus, we will define, study and characterize, for the first time, column-compound
161 extreme events in the vertical water column at the global scale, and aim to understand
162 their drivers. To this end, we will use results from a hindcast simulation undertaken with
163 a global ocean coupled physical/biogeochemical model, sampled at high temporal fre-
164 quency to permit us to identify extremes. We rely on model simulation results since there
165 are no observational records available across all parameters and especially not at depth
166 that would permit us to undertake this study based on observations.

167 We also develop a framework to analyze such events, which we call Column-Single
 168 eXtreme events (CSX) in the case of a single parameter being extreme across a good por-
 169 tion of the water column, and Column-Compound eXtreme events (CCX), which are those
 170 events when more than one CSX is detected in the same column at the same time. We
 171 will show that these events are prevalent in the ocean, although primarily occurring in
 172 the low latitudes, and that their frequency, duration, and intensity have increased in re-
 173 cent decades. While we cannot identify the potential impacts yet of these extremes on
 174 marine organisms and ecosystems, the multi-dimensional nature of the extreme condi-
 175 tions are bound to push marine organisms to their limits. We will show the places and
 176 times where these column extremes tend to occur, giving insights into where and when
 177 one should look for these ecological impacts.

178 2 Detecting Extreme Events in the Water Column

179 No consistent definition of single or compound marine extreme events exists so far,
 180 much less if they are co-occurring in the same vertical column. We thus first review the
 181 issues at hand, and then illustrate the framework we have used to identify the Column-
 182 Single eXtreme events (CSX) and the Column-Compound eXtreme events (CCX).

183 A common issue to be resolved in all studies is the choice of thresholds and base-
 184 lines. Regarding the threshold, the MHW-related studies have relied on a relative per-
 185 centile threshold approach with the majority of studies using a seasonally-varying (Oliver
 186 et al., 2018; Holbrook, Sen Gupta, et al., 2020), so that extreme conditions can be de-
 187 tected regardless of the season. In contrast, absolute thresholds remain pertinent to ex-
 188 tremes such as LOX, where the metabolic requirement for organisms tends to be fixed
 189 (Hofmann et al., 2011), with some degree of variability with temperature (Seibel, 2011;
 190 Deutsch et al., 2015). Absolute thresholds have also been used to detect extremes in arag-
 191 onite saturation state (Hauri et al., 2013; Negrete-García et al., 2019; Desmet et al., 2022),
 192 where a thermodynamic threshold determines the state of dissolution of the shells of cal-
 193 cifying organisms. Thus, there are clear grounds for using either relative or absolute thresh-
 194 olds, and we make use of both in this study.

195 The baseline, i.e., the time-period used to identify the thresholds, is also a criti-
 196 cal choice in detecting extremes (Jacox, 2019; Oliver et al., 2021; Sen Gupta, 2023). In
 197 the case of a fixed baseline, the thresholds remain invariant such that the trends in tem-
 198 perature, pH, and oxygen imply an increase in the frequency and intensity of extremes
 199 events (Gruber et al., 2021). This could be problematic when cold spells in later years
 200 are potentially marked as heatwaves (Jacox, 2019), or when waters become classified as
 201 permanently extreme with regard to ocean acidification (Hauri et al., 2013; Burger et
 202 al., 2020, 2022; Gruber et al., 2021). An alternative is the use of a moving baseline, i.e.,
 203 where the reference period used to identify the relative thresholds is shifting in time with
 204 the analysis, or alternatively, where the thresholds are computed based on detrended data.
 205 An analysis with such a moving baseline gives equal weight to extreme events across the
 206 entire time period (Burger et al., 2020; Rosselló et al., 2023), and is more suitable for
 207 the investigation of drivers (Chiswell, 2022). It is also more relevant to organisms that
 208 are able to adapt to the gradually changing conditions (Holbrook, Sen Gupta, et al., 2020;
 209 Oliver et al., 2021), but are still affected by the sudden change in conditions during an
 210 extreme event. In this study, we first present our results on a fixed baseline, illustrat-
 211 ing the response of extreme events to the climate trend. Then, we primarily use the mov-
 212 ing baseline to analyse extreme events and postulate drivers. A quadratic moving base-
 213 line is chosen to fit the long term trend in H^+ (Hauri et al., 2021) (Supporting Infor-
 214 mation Text S1 and Figure S1-S2).

215 The next choices concerns the vertical structure and the compounding. For the ver-
 216 tical structure, we define columns to be Column-single eXtreme events (CSX) of a par-
 217 ticular type (MHW, OAX, or LOX) when the grid cells that are considered to be extreme

with regard to this particular parameter occupy more than 50 m of the upper 300 m of the water column. For the compounding, we identify columns to be Column-Compound eXtreme events (CCX) when more than one CSX is detected in the same column at the same time. This leads to three types of double stressor CCX, i.e., MHW-OAX, MHW-LOX, and OAX-LOX, and one type of triple stressor CCX, i.e., MHW-OAX-LOX.

In Figure 1a, a conceptual sketch of the various types of defined extremes is shown for a single column over time. Grid-cell extreme events are coloured within the Hovmoller diagram where they occur. However, this does not mean that a column extreme is occurring. For example, a CSX-MHW starts at day 20 from the surface, while a CSX-OAX and CSX-LOX start from the bottom of the column at days 35 and 47 respectively. The duration of the CSXs and CCXs are labelled with arrow ranges below Figure 1b.

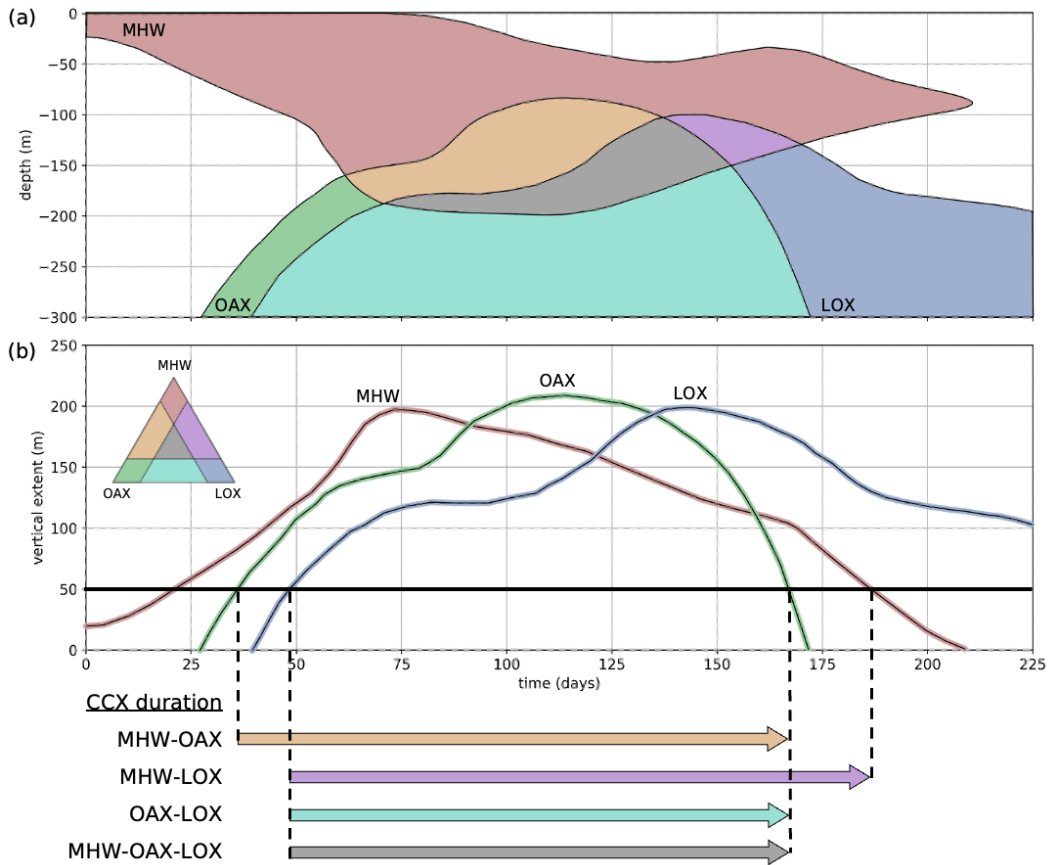


Figure 1. Illustration of the concepts used to detect and analyze column compound extremes. (a) Idealized Hovmoller diagram illustrating the time-depth evolution of extreme conditions in a hypothetical water column from the surface down to 300 m depth. The coloured regions within the plot are considered extreme, with the colors brown, green and blue representing pure MHW, OAX and LOX, respectively. The areas where the different extremes overlap are given colors according to the mixing diagram in panel (b). (b) Timeseries of the total vertical extent (within the top 300 m of the water column) for each extreme type. When the vertical extent for a particular type of extreme exceeds 50 m, then we call it a *Column-single eXtreme event* (CSX) of this parameter and when more than one of these occur at the same time a *Column-Compound eXtreme event* (CCX). The duration of the four different types of CCX is indicated by arrows.

3 Methods

3.1 Model Simulations

To identify the CSX and CCXs, we use results from a hindcast simulation performed with the ocean component of the global Community Earth System Model (CESM) Version 1.2 (Gent et al., 2011). The ocean component consists of the Parallel Ocean Program 2 (POP2) (R. Smith & Gent, 2010) simulating ocean circulation and mixing, of the Community Ice Code 4 (CICE4) model, also known as the Los Alamos Sea Ice Model (Hunke & Lipscomb, 2008) simulating the presence and thickness of sea-ice, and of the Biological Elemental Cycling (BEC) model (Moore et al., 2004, 2013) representing ocean ecology and biogeochemistry. The model has a nominal meridional resolution of 0.5° near the poles, refining to 0.3° at the Equator, and a nominal zonal resolution of 1° . There are 60 depth levels in the vertical dimension, extending from the surface to 5375 m. BEC includes three phytoplankton functional types that are grazed by one zooplankton type. The temperature and dissolved oxygen fields are prognostic variables of the coupled model, while the hydrogen ion concentration (on the total scale) values were obtained from the model simulated inorganic carbon parameters by applying carbonate system calculations based on the OCMIP2 routines (Orr et al., 2005). Details of the model can be found in S. Yang and Gruber (2016).

The model simulations started from a spun-up preindustrial state (S. Yang & Gruber, 2016) and was brought forward from 1850 to 1957 with cyclically repeated monthly atmospheric forcing from the Japanese 55-year Re-analysis (JRA-55) product (Ebita et al., 2011) and atmospheric CO_2 prescribed according to observations provided by the Global Carbon Project (Friedlingstein et al., 2022). The hindcast simulation was then produced with daily output for the years 1958 to 2020 also using the monthly JRA-55 forcing. We discard the first three years, and thus limit our analysis to the 60-year period between 1961 and 2020. Results from this simulation were also used for the global Carbon Budgets 2020 and 2021 (Friedlingstein et al., 2022) and in the study by Hauck et al. (2020).

3.2 Extreme Events Detection

In the first step, single extreme events of MHW, OAX, and LOX are detected for each grid cell for each day. For MHW and OAX, a 95th percentile threshold is applied to the temperature and H^+ fields respectively, using seasonally varying thresholds. For LOX, we require the oxygen concentration to be below the 5th percentile value (again seasonally varying), and simultaneously to be less than $150 \mu\text{M}$ ($\sim 3.5 \text{ ml/L}$). The absolute threshold for LOX was added because LOX at high oxygen levels have very little biological impact. The value chosen is the hypoxic threshold of some larger fish species such as yellowfin and skipjack tuna, marlin, and sailfish (Braun et al., 2015; Leung, Milan, et al., 2019; Rose et al., 2019). The detection thresholds for single events in the grid cell are summarised in Table 1. In this work, we do not impose any additional criteria such as minimum duration (Hobday et al., 2016), since the monthly forcing applied to the CESM hindcast prevents the formation of short duration events that may have to be filtered out. For the fixed baseline thresholds, the data are detrended with a quadratic trend to a reference year of 1958 prior to computing the percentile thresholds. For the moving baseline results, the thresholds change with time with respect to the fitted quadratic trend.

Table 1. Single extremes and the thresholds used for their detection

Single Extreme Type	Variable	Percentile Threshold	Additional Absolute Threshold
Marine Heatwave (MHW)	T	> 95 th	-
Ocean Acidification Extreme (OAX)	[H ⁺]	> 95 th	-
Low Oxygen Extreme (LOX)	[O ₂]	< 5 th	< 150 μ M

274 To define extreme events in the vertical column, we require at least 50 m out of the
275 top 300 m to be extreme with respect to each stressor. The analysis range of 300 m re-
276 flects the vertical habitat range of epipelagic and other vertically migrating organisms
277 (Bertrand et al., 2010; Bianchi et al., 2013; Bianchi & Mislán, 2016). The value of the
278 minimum extension of 50 m is somewhat subjective, but aims to capture the occasion
279 when a substantial fraction of the water column is extreme, affecting the organisms liv-
280 ing within this water column in a major way. Adjusting this minimum extension mod-
281 ulates the number of column extremes detected, but does not significantly change their
282 spatial or temporal distribution (Supporting Information Test S2 and Figures S3-S6).
283 When the 50 m vertical threshold is met for a single stressor, it is denoted as a column-
284 single extreme event (CSX), illustrated in Figure 2a. The criteria for a CCX is met when
285 two or more CSXs occur in the same vertical column, at the same time. Various con-
286 figurations of CCXs are illustrated in Figure 2b. CSXs can be separately located in the
287 column (c), or have some overlap (e). The single extreme grid cells do not need to be
288 connected vertically to meet the 50 m threshold, as seen in (b) and (d). Under our def-
289 inition of CCXs, triple compound events of MHW-OAX-LOX are also always double CCXs,
290 and are included in their metrics.

291 3.3 Extreme Event Metrics

292 The metrics used to characterise extreme events can be broadly grouped into fre-
293 quency, intensity, and temporal categories. With regard to extremes in the vertical col-
294 umn, we also quantify their size, location, and remaining continuous habitable space (see
295 Table 2). While many of these metrics are commonly used in extreme studies, some had
296 to be redefined in the context of our work on column extremes. We do not include sever-
297 ity in our analyses, i.e., the cumulative sum of the intensity value over the duration of
298 the event (Hobday et al., 2016; Hauri et al., 2013; Samuels et al., 2021) since it strongly
299 correlates with the event duration.

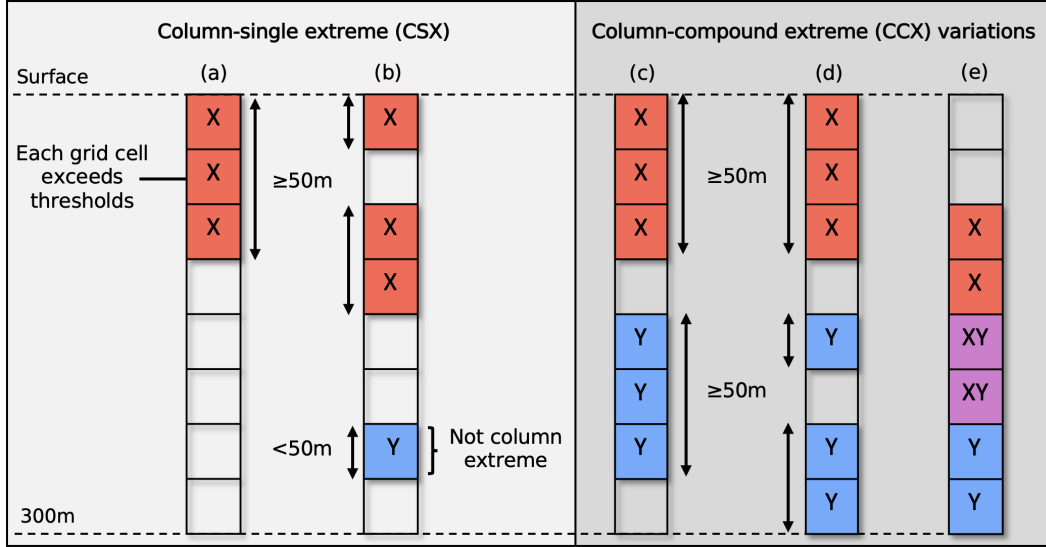


Figure 2. Illustration of different types of column-extreme events within the water column. (a) Column-single extreme (CSX), (b) CSX with discontinuous grid cells of extreme type 'X', (c) Column-compound extreme (CCX), (d) CCX with discontinuous grid cells of extreme type 'Y', (e) CCX with overlapping 'X' and 'Y' type extremes.

Table 2. Metrics used in the analysis of extreme events

Name	Symbol	Definition
<i>Frequency metrics</i>		
Days per year	N	Mean number of extreme days per year
Co-occurrence propensity	CP	Likelihood of two or more CSXs occurring within the same vertical water column at the same time
Enhancement (Suppression) of CCX during ENSO	ΔN	Mean increase (decrease) in number of extreme days per year during ENSO events, compared to that in the neutral phase
<i>Intensity metrics</i>		
Intensity index	ψ_i	Ratio of an event variable's i difference from its climatological value to the difference between the threshold and climatological value
Compound intensity index	Ψ	Square-root of the sum of squares of the intensity index of individual events, that make up a compound event
Maximum intensity index	ψ^{\max}	Maximum value of the intensity index over time and the vertical column
<i>Temporal metrics</i>		
Duration	D	Lifetime of an event for which the thresholds are met continuously
<i>Size and location metrics</i>		
Volume fraction	f_V	Fraction of total volume of a defined region that is affected by the specified extreme type
Vertical fraction	f_z	Fraction of top 300 m occupied by extremes
Contiguous habitable space fraction	f_h	Fraction of the top 300 m continuously unaffected by extremes

300 The duration of an event refers to the total length of time for which the specified
 301 extreme type exists in the water column. For example, a MHW-OAX event starts from
 302 the time CSX-MHW and CSX-OAX both exist in the water column, even if the CSX-
 303 MHW started earlier (see Figure 1). The same applies to the end of a CCX.

304 The intensity index expresses the strength of a extreme event in a unitless fash-
 305 ion. It is inspired by the MHW categories of Hobday et al. (2018), and defined as the
 306 continuous severity index by Sen Gupta et al. (2020). Using the intensity index as a mea-
 307 sure of event intensity permits us to compare the intensities of multiple extreme and even
 308 to combine them. For a single grid cell it is expressed as:

$$\psi_X = \frac{X - X_c}{X_t - X_c}, \quad (1)$$

309 where X is the parameter of interest, X_c is its climatological value for that day of the
 310 year, and X_t is the threshold value. For the climatology, we use the median value in or-
 311 der to prevent it from being skewed by exceptionally intense extreme events. Th median
 312 value is obtained from a seasonally-varying 11-day rolling window. To express the in-
 313 tensity index of a multiple extremes occurring in the same grid cell, we take the Euclidean
 314 norm of ψ of the single extremes:

$$\Psi = \sqrt{\psi_X^2 + \psi_Y^2 + \psi_Z^2}, \quad (2)$$

315 where ψ_X , ψ_Y , and ψ_Z are the intensity index values of single extremes.

316 The co-occurrence propensity (CP) is a central metric for the study of compound
 317 extremes as it permits us to assess whether two extremes co-occur by chance, or whether
 318 they co-occur as a result of a common process forcing them. Likewise the propensity can
 319 be used to assess whether two extremes co-occur much less frequently than expected by
 320 chance, since the common process actually leads to conditions that suppress the co-occurrence.
 321 The CP metric is defined as the likelihood of two (or three) different CSXs occurring
 322 in the vertical column at the same time. It is scaled to the range of $[-1,1]$. A value of 1
 323 indicates the CSXs always occur together whenever they occur, while a value of -1 in-
 324 dicates that they never occur together. A value of 0 suggests that their occurrences are
 325 independent, as if randomly distributed in time. A high value suggests that the CSXs
 326 in consideration have similar or related drivers, while a low value suggest that they have
 327 opposing drivers. The CP metric is similar in concept to the likelihood multiplication
 328 factor (Zscheischler & Seneviratne, 2017).

329 First, the independent (random) value of CCX days per year is computed using the
 330 mean number of CSX days per year:

$$N_r = \begin{cases} \frac{N_1}{D_Y} \frac{N_2}{D_Y} \times D_Y, & \text{for double extremes,} \\ \frac{N_1}{D_Y} \frac{N_2}{D_Y} \frac{N_3}{D_Y} \times D_Y, & \text{for triple extremes,} \end{cases} \quad (3)$$

331 where N_1 , N_2 , N_3 are the mean number of days per year of different CSXs, and $D_Y =$
 332 365 is the number of days in a year. The CP metric is then defined as:

$$CP = \begin{cases} \frac{N - N_r}{N_{\max} - N_r}, & N > N_r \\ \frac{N - N_r}{N_r}, & N < N_r \\ 0, & N_r = 0 \end{cases} \quad (4)$$

where N is the mean number of days per year of the CCX, and N_{\max} is the global maximum value of N . Since CP is proportional to the mean number of days of extremes, it is also representative of the annual number of days.

3.4 Clustering of Extremes

In order to find commonalities of the detected CCXs with regard to their vertical structure and to assist us in identifying the underlying drivers, we cluster the detected CCXs with a k-means clustering approach (MacQueen, 1967). The clustering algorithm is performed on the vertical locations of single extreme events in the column, exclusively during CCXs and for grid cells with a positive co-occurrence propensity. In detail, the water column is first divided into 6 bins of 50 m each, and then, over the 60 year analysis period the number of occurrences of single extremes in each bin during CCXs is counted and weighted with their intensity index. These bins of vertical locations are then used as the dimensions of the clustering, with 12 dimensions for the double CCXs, and 18 dimensions for the triple CCX. These dimensions are chosen as the vertical locations of single extremes reflect the conditions under which they occur, and allude to their drivers. Further information about the clustering approach and choice of number of clusters is provided in the Supporting Information Text S3 and Figure S10.

3.5 Model Evaluation

Given our relying on model simulation results for detecting single and compound extremes across the upper water column, it behooves us to evaluate the model with regard to its ability to represent extremes. But our evaluations are largely limited to the surface. For MHW, we use the observations of sea-surface temperature from the Operational Sea Surface Temperature and Sea Ice Analysis (OSTIA) product (Good et al., 2019, 2020), covering the period 1982 to 2020. For OAX, we rely on the OceanSODA-ETHZ dataset (Gregor & Gruber, 2021) that covers the period 1982 to 2020. Surface MHW and OAX are detected in the monthly means of the observational products with a seasonally-varying 95th percentile threshold on a quadratic moving baseline, analogous to how this was done for the model output (see section 3.2). As ENSO turns out to be a major driver for the variability in extremes, we evaluate the model also with regard to ENSO, using the Oceanic Niño Index (ONI) and the depth of the 20°C isotherm across the equatorial Pacific.

The model captures the observed variations and global coverage of surface MHWs with high fidelity (Figure 3(a)). In particular, the model captures well the strong year-to-year fluctuations, which tend to be closely coupled to ENSO. The model also correctly simulates the distribution of the mean duration of these surface MHWs, especially the long MHW durations found in the eastern tropical Pacific. However, there is a slight tendency for the model to overestimate the duration, particularly in the extratropics (Figure 3(b)). This is common shortcoming of models (Frölicher et al., 2018; Gruber et al., 2021; Köhn et al., 2023) and while there are clearly issues with the models, it is also feasible that the observations tend to underestimate the duration owing to observational gaps. Finally, the model also represents the intensities of the surface MHW with great fidelity, both with regard to the absolute values and distribution (Figure 3(b)). We thus concluded that the model is performing very well with regard to the representation of the large and long-duration MHW at the surface.

The evaluation of surface OAXs with the observation-based product OceanSODA-ETHZ (Gregor & Gruber, 2021) produces somewhat more mixed results. However, one needs to note that the uncertainties associated with this product are much larger than those associated with SST. This is a consequence of the several orders of fewer observations that are available to construct a space-time distribution of pH or $[H^+]$. Still, the model-based timeseries of the global area coverage of surface OAX (based on $[H^+]$) agrees

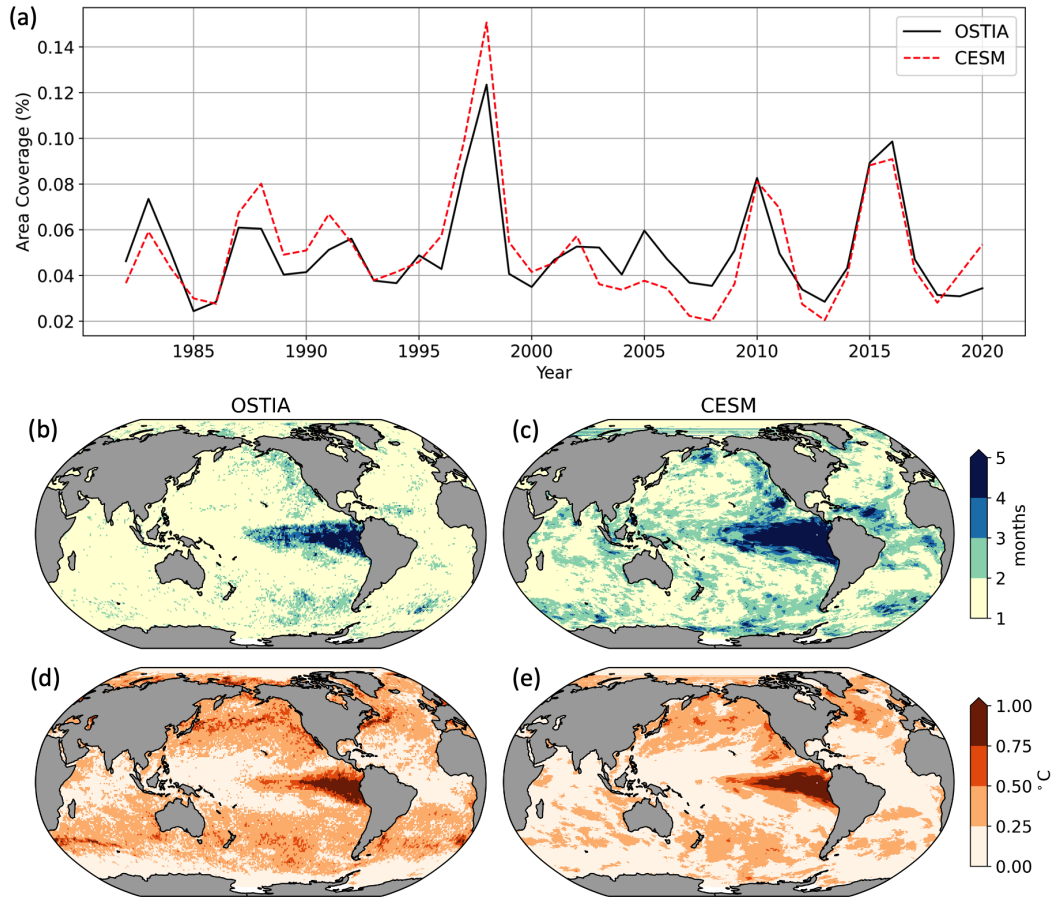


Figure 3. Evaluation of the hindcast model CESM with regard to its representation of surface marine heatwaves (MHW). (a) Timeseries of annual global area coverage of surface MHW identified by the OSTIA observational product compared to those diagnosed in the CESM hindcast. (b) OSTIA and (c) CESM mean duration of surface MHW. (d) OSTIA and (e) CESM mean annual maximum MHW intensity. The MHW were diagnosed in the observations in the same manner as done for the model.

383 remarkably well with that inferred from the observation-based product, both in terms
 384 of mean and year-to-year variations (Figure 4(a)). However, the peak values differ by
 385 up to about 50%, with this difference being especially apparent in the years 1988-1989
 386 and 1997. The surface OAXs detected with CESM have a similar pattern as that inferred
 387 from the observation-based product, especially with regard to the locations of the longest
 388 and most intense OAXs that are found in the tropical Pacific (Figure 4(b) and (c)). How-
 389 ever, there is a mismatch in the high latitudes, especially in the North Pacific and South-
 390 ern Ocean, where the model identifies long-lasting and intense surface OAX events, while
 391 they are not detected in the observation-based product. We suspect that this difference
 392 is most likely a consequence of the observation-based product underestimating the vari-
 393 ability of $[H^+]$, thus detecting fewer and less intense OAXs. It also might be a consequence
 394 of biases in the model. Regardless, biases in the intensity tend to have only a minor effect
 395 on most conclusions drawn in this study, especially not with regard to the propen-
 396 sity or the mechanisms. Biases in intensity will impact, though, any derived metric, such
 397 as the compound intensity index of compound-OAX events.

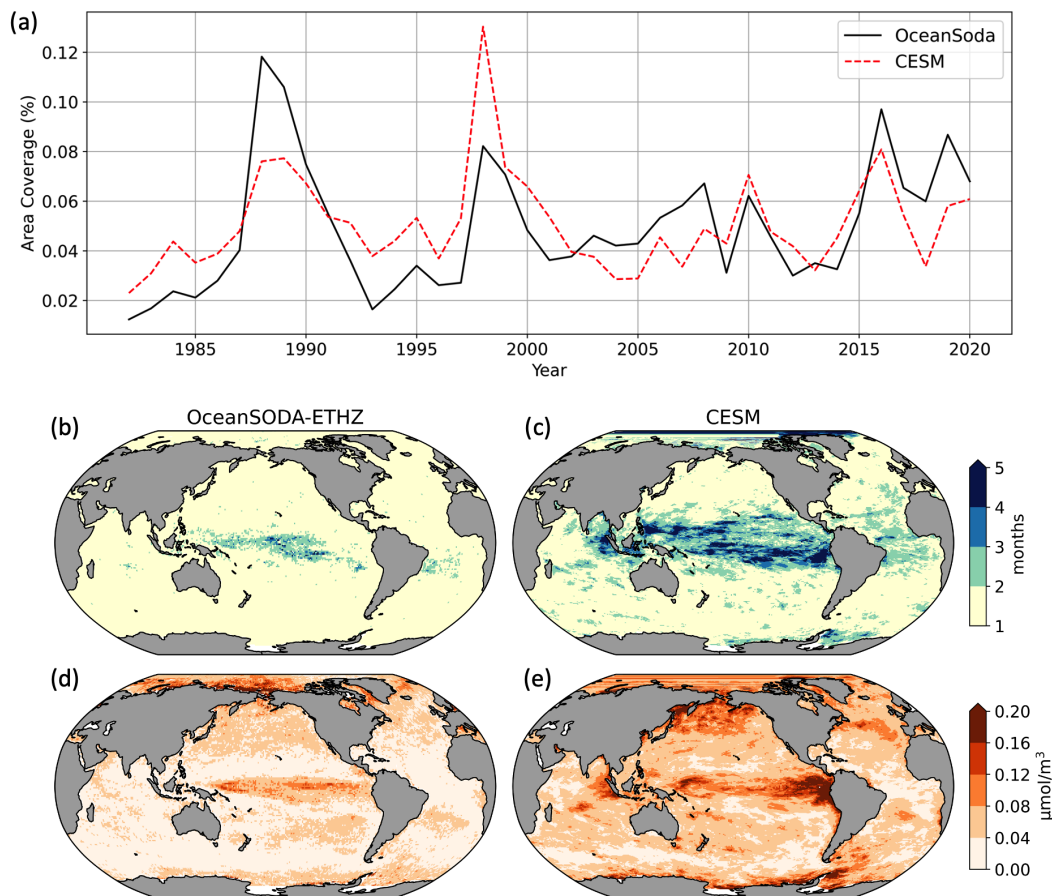


Figure 4. Evaluation of the hindcast model CESM with regard to its representation of surface ocean acidification extreme events (OAX) (a) Time-series of annual global area coverage of surface OAX identified on the basis of the OceanSODA-ETHZ observational product (Gregor & Gruber, 2021) compared to those diagnosed in the CESM hindcast. (b) OceanSODA-ETHZ and (c) CESM mean duration of surface OAX. (d) OceanSODA-ETHZ and (e) CESM mean annual maximum OAX intensity.

398 The hindcast model is doing an excellent job in simulating not only the time-series
 399 of the Oceanic Niño index ONI (bias of $0.11\text{ }^{\circ}\text{C}$, and correlation coefficient of $R^2 = 0.91$,
 400 based on ORAS5 (Zuo et al., 2019)), but also the variation of the thermocline structure
 401 in the eastern Pacific. Concretely, we assess the ability of the model to reproduce the
 402 depth of the $20\text{ }^{\circ}\text{C}$ isotherm at monthly resolution (Supporting Information Figure S7).
 403 The interannual variability of the isotherm depth is comparable between the two, and
 404 the time scales of ENSO events are similar. We find a weaker zonal gradient in the CESM
 405 hindcast during ENSO events. This is likely due to a dampening of its SST variability
 406 due to a lower spatial resolution and monthly atmospheric forcing. But we overall con-
 407 clude that the hindcast model is able to capture not only the mean state of the ocean’s
 408 physical and biogeochemical state, but also its variability, which is a critical require-
 409 ment to investigate extremes.

4 Results and Analysis

4.1 Trends of Column Extremes

Our model simulations reveal that the volumes occupied by column extremes for single parameters, i.e., CSXs and particularly those for OAX and MHW, have increased substantially over the 60 years of our analysis (Figure 5a). Their volume fractions started from values of a few percent in the 1960s and doubled for LOX, more than quadrupled for MHW to more than 20%, and reached nearly 100% for OAX by the end of the simulation in 2020. As these metrics were computed with a fixed baseline reflecting the conditions of the 1950s, these increases are a direct consequence of the underlying changes in temperature, oxygen, and acidity. The rapid changes in OAX and the more moderate increases in MHW diagnosed for the column extremes mimic the results obtained for the surface (Oliver et al., 2018; Burger et al., 2020; Gruber et al., 2021). This reflects the fact that ocean warming and ocean acidification are not limited to the surface, but are extending over much of the upper ocean (Gleckler et al., 2016; Kwiatkowski et al., 2020), causing strong trends also in column extremes. The trend in LOX events are comparatively muted because of smaller trends in oxygen and because of the additional absolute threshold of $150\ \mu\text{M}$ used in this study.

The increasing volume fraction of single parameter CSXs causes also the volume fraction of column compound extremes (CCX) to increase, but the increases are less steep and also not as monotonic (Figure 5b). In the 1960s and 1970s, the volume fractions of the different combination hover around 0.1-1%, with the OAX-LOX events being the most prevalent at around 1%, and the triple compound extreme occupying less than 0.1% of the water column, on average. But then at various points in time, the prevalence of these CCX suddenly increased, such as is the case for the MHW-OAX extremes around 1980, from where the volume fraction increased to almost 25 % in 2020. The volume fraction of OAX-LOX jumped up around 1995, and then remained fairly constant near 5 %. The smallest increases are seen for the volume fraction of MHW-LOX and MHW-OAX-LOX, but they still increased by 2 and 24 times when comparing the first and last 20 years.

As the volume of CCXs has increased over the last 60 years, their duration has increased as well (Figure 5c). MHW-OAX and OAX-LOX events lasted on average less than 50 days before ~ 1995 , but jumped up in 1997. Thereafter, the mean duration of these CCXs rarely fell below 50 days and instead, achieved new records with durations of close to 200 days. MHW-LOX and the triple compound events have also increased in duration over the hindcast period, averaging close to 50 days per event towards 2020.

The starkest changes in the CCX properties occurred with the maximum intensity index (Figure 5d). In the 1960s and 1970s, it hovered around 2 for all compound extremes, except for OAX-LOX. But then, as the intensity of the OAX began to increase rapidly owing to the strong trends in ocean acidification (Ma et al., 2023), the maximum intensities of all CCX began to increase rapidly as well, reaching a nearly 10 fold increase by 2020. The exception are the MHW-LOX, which experienced "only" a doubling in their maximum intensity.

In summary, column compound extremes used to be relatively rare, but have become much more prevalent and frequent over the last few decades, and, in particular, have become much more intense. This is best illustrated for the triple column compound extremes that have expanded 24-fold, now last 3-times longer, and have become 6-times more intense since the early 1960s. The 0.45% of the volume of the global upper ocean being under conditions of triple compound extremes in recent years corresponds to $450\ \text{km}^3$ of the ocean. This is much larger than e.g., the volume of the ocean that is considered "dead" as a consequence of coastal eutrophication (Diaz & Rosenberg, 2008). Thus, while many studies have already shown the increasing frequency, duration, and intensities of surface extremes, especially those of MHW, our work now shows that this leads to se-

Fixed Baseline

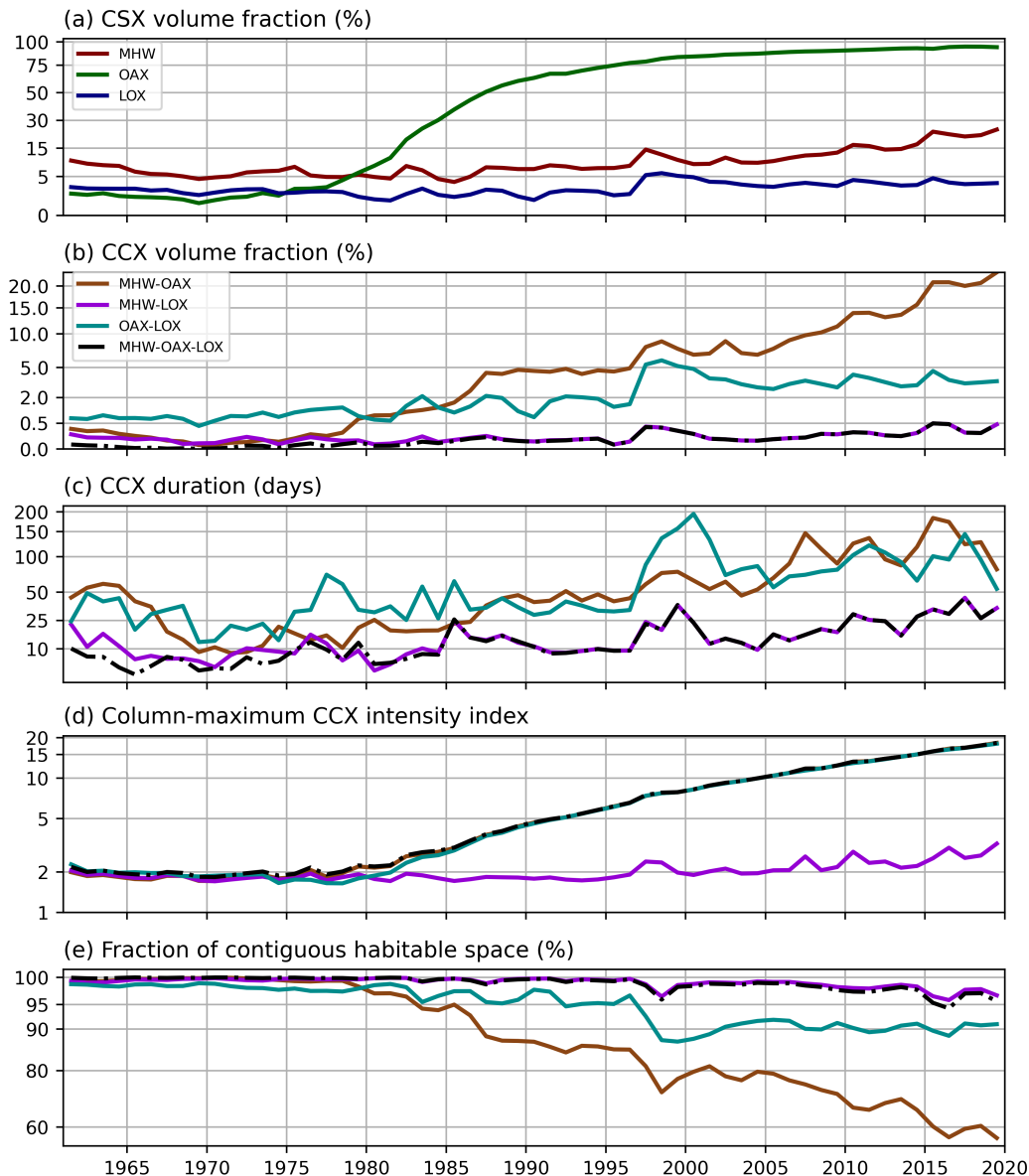


Figure 5. Temporal evolution of model simulated column extremes over the past 60 years on a fixed baseline. Shown are the timeseries of (a) annual mean global volume fraction of the three single column extremes (CSX), (b) annual mean global volume fraction of column compound extremes (CCX) of the four different types, (c) mean CCX duration, and (d) annual column-maximum CCX intensity index.

461 vere reductions in habitable space below the surface, restricting the capability of organ-
 462 isms to cope with e.g., surface MHW by by migrating to deeper depths. These analy-
 463 ses also show how important it is to better understand the impact of compound extremes
 464 on marine organisms, as these compound extremes are getting common.

465 Next, we would like to investigate the processes behind these events, and also un-
 466 derstand what causes, e.g., also the strong year-to-year variations in the trends. We also

would like to characterize the events more specifically with regard to where they occur and what properties they have. To this effect, we change our perspective to a moving baseline which removes the long-term trend. We do this without the intention of understating the increasing severity of marine extremes under climate change.

4.2 Temporal Variability of Column-Compound Extremes

By removing the underlying climate trend through the use of a moving baseline, the strong year-to-year variability of the column-compound extremes become clearer (Figure 6). In particular, local peaks in global volume fraction, duration, and intensities of CCX coincide with ENSO events of high Oceanic Niño index (ONI). Most visible are the alignments of the peaks during moderate and strong ENSO events in 1972-1973, 1982-1985, 1997-1998, 2009-2011, and 2015-2016. In the tropical Pacific, we find that the volume fraction of double CCXs has a high Spearman correlation coefficient of >0.72 with El Niño events ($|\text{ONI}| > 0.5^\circ\text{C}$, indicating that these events are likely to be driven by El Niño). The triple compound extremes have a lower correlation of 0.33 with El Niño. With La Niña, we find an asymmetric relationship with CCX volume fraction as compared with El Niño, with relatively weaker correlations. The highest coefficients of 0.37 and 0.35 are found for the triple CCX and for MHW-LOX, respectively, reflecting also the high interannual correlation of the triple CCX with MHW-LOX. OAX-LOX is correlated with La Niña with a coefficient of 0.26, while MHW-OAX does not demonstrate any significant correlation. While ENSO can be identified as a major driver for many CCXs, especially in the tropical Pacific, it is also correlated with CCXs in other parts of the globe. We look into the correlation on a regional scale in Section 4.5.

OAX-LOX events affect the water column more than any other type of CCX. On average, they have the highest volume fraction of 0.73% (735 km^3), reaching up to 3% (3000 km^3) during the strong consecutive El Niño/La Niña events of 1997-1998. They also have the longest duration, lasting about 18 days on average, but exceeding 40 days during some periods. Due to their large volume, they also contract the habitable space the most out of all the CCX types.

The second most extensive type of CCX is MHW-OAX occupying typically about 0.3% of global volume (280 km^3), and lasting 11 days on average. Together with the triple CCX, they are also one of the most intense CCX types, with an intensity index typically close to 2. While some peaks may be seen coinciding with major ENSO events, their association with ENSO is weaker than that of OAX-LOX. Finally, there is a relatively smaller volume of MHW-LOX and the triple CCX (MHW-OAX-LOX) during most years, of 0.038% and 0.012% respectively, corresponding to 38 km^3 and 12 km^3 . These two CCX types have the same interannual variability, suggesting that many MHW-LOX events are also triple compound events.

4.3 Spatiotemporal Distribution of Column-Compound Extremes

The four different types of CCXs have a rather different global distributions in terms of the annual CCX days, i.e., the average number of days per year a particular location is characterized as a CCX (Figure 7a,c,e,g), and in terms of the co-occurrence propensity (Figure 7b,d,f,h). MHW-OAX occur globally, but most frequently in the subtropics and the high latitude Southern Ocean where typically about one week per year is characterized by a MHW-OAX event. In contrast, the number of MHW-OAX extreme days in the equatorial regions is low, and typically less than a week. The OAX-LOX events have nearly the opposite pattern. They occur primarily in the tropics, in the EBUS, and the north sub-polar Pacific with typically more than two weeks per year being under CCX conditions. No OAX-LOX CCX are detected in the North Atlantic and the ocean south of about 30°S . Compared to these first two CCX types, the MHW-LOX and the triple compound occur substantially less often, and last typically less than 7 days. The spa-

Moving Baseline

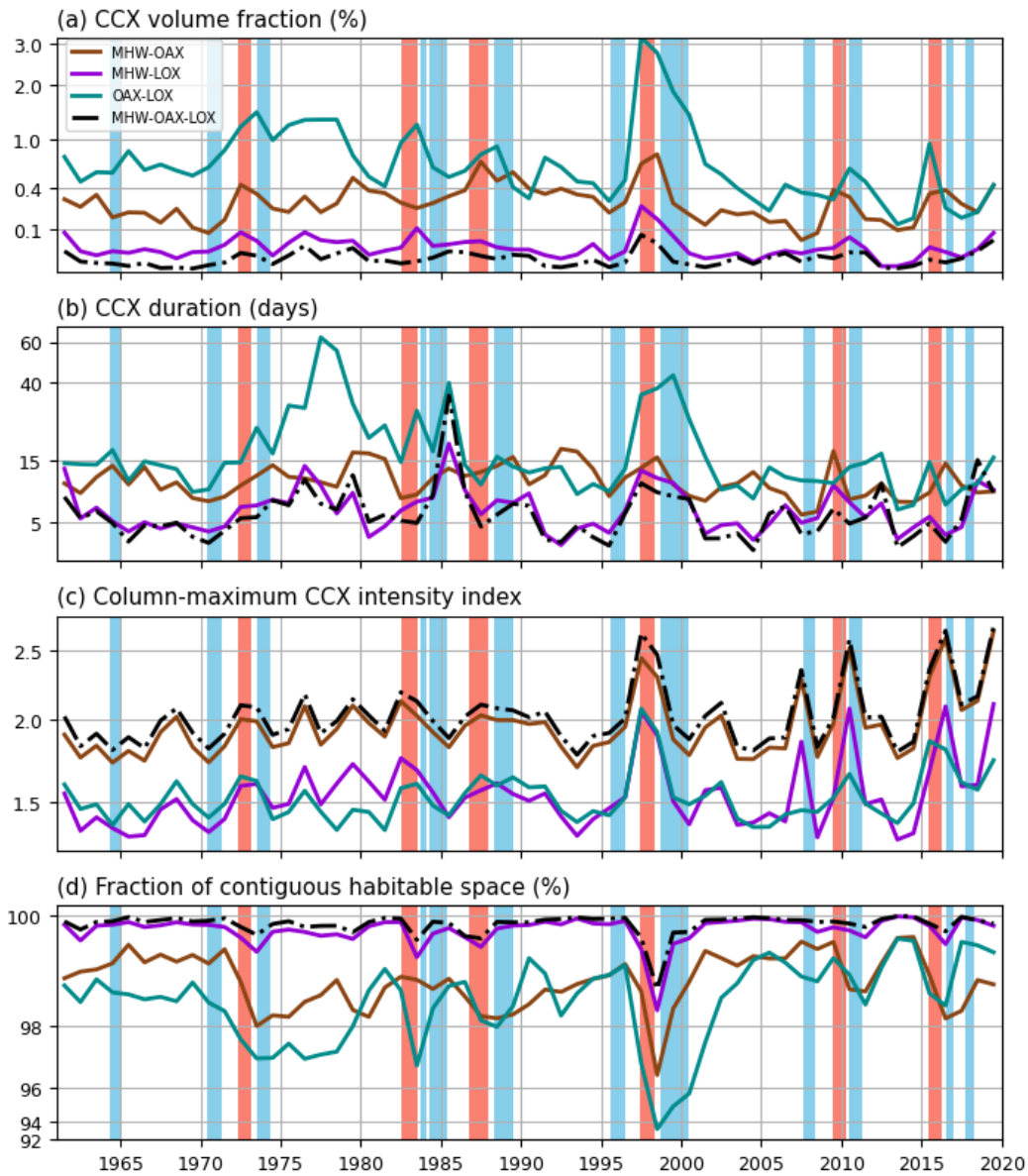


Figure 6. As Figure 5, but for a moving baseline, i.e., when the trends are removed using a quadratic fit. Strong El Niño events ($\text{ONI} \geq 1.5^\circ\text{C}$) are shaded in red, and strong La Niña events ($\text{ONI} \leq -1.0$) are shaded in blue.

517 tial pattern is similar to that of the OAX-LOX extremes with a low-latitude focus. Their
 518 similar distributions are due to the close association of OAX with LOX, such that a ma-
 519 jority of MHW-LOX are also MHW-OAX-LOX.

520 The co-occurrence propensity (later referred to as just propensity) helps to explain
 521 elements of these distributions. For example, the strongly negative propensity of the MHW-
 522 OAX events in the eastern tropical Pacific explains well why the number of CCX days
 523 in this region is so low (Figure 7a,b). This negative propensity means that whenever there
 524 is e.g., a heatwave in this region, the likelihood that this region has also an OAX is sub-

stantially lower than by chance. This can occur, for example, when heatwaves suppress the formation of OAX events. The very positive propensity for the OAX-LOX extremes in the tropics helps also to understand the high number of extreme days there. This means that when the region is characterized by either one of the two extremes, the likelihood of the other occurring is much higher than by chance. This can occur when the processes governing the development of these extremes are closely coupled. The much lower number of extreme days for the MHW-LOX and the triple compound extremes is also a consequence of the many regions with very negative propensity.

Thus, we can identify two overall patterns of CCX occurrence and propensity. A more global and high latitude pattern for MHW-OAX extremes, and a more low latitude/tropical pattern for the other three CCX types. This permits us in the following discussion of the full sets of metrics of the CCX to focus on just two of the four types, i.e., the MHW-OAX events (Figure 8) and the MHW-OAX-LOX triple compounds (Figure 9). The figures for the other two CCX types, i.e., OAX-LOX and MHW-LOX may be found in the Supporting Information Figures S8-S9.

MHW-OAX events in the subtropics and Antarctic zone last the longest (more than 21 days) (Figure 8a). In these regions we also see the highest intensity index of 2 to 4 (Figure 8b), which means that the intensity of combined events are roughly 2 to 4 times the intensity of the threshold. This shows that where MHW-OAX occurs most frequently, they are also long and intense. Likewise, in the tropical regions where the number of CCX days is small and where the CCX events are short (Figure 8a, c) they are also relatively weak. This is also the region of very low propensity (Figure 8d). But when the CCX events are frequent, long and intense, they contract the habitable space moderately, between 25 % to 75 % of the column (Figure 8e). Meanwhile we see the highest contraction in the tropics between 50 % and 100 % of the column.

The spatial distribution of the triple compound event (MHW-OAX-LOX) can be understood in conjunction with that of OAX-LOX. OAX-LOX is unique from the other CCX types due to its high number of days per year (Figure 7c), and positive propensity everywhere it occurs (Figure 7d). This means that when either OAX or LOX occurs, the other almost always occurs together with it. The triple compound thus occurs when a MHW is induced in the same column. We see this most frequently in the tropics and the Bering sea, up to 21 days per year in some areas (Figure 9c). When they occur, they typically have moderate intensity index of 2 to 3, but exceeds 4 in the central tropical Pacific (Figure 9b). In the equatorial regions, they typically last up to 10 days (Figure 9c). However, their durations are more than double in the Bering sea and on the boundaries of the subtropical gyres. By far the triple compound event contracts habitable space the most (Figure 9f), by at least 50 % everywhere, and close to 100 % in some areas.

The key metrics for all the other events may be found in the Supporting Information (Figure S8-S9).

4.4 Vertical Structure and Clustering of CCXs

Next, we use the results of the k-means clustering of the CCXs in order to identify commonalities across the global ocean, helping us also to link the occurrence with potentially underlying processes. In the clustering, only those regions with a positive co-occurrence propensity were considered, i.e., where the likelihood of occurrence was larger than by chance (Figure 7). Even though the only information used for the clustering was the vertical distribution of the extremes, the resulting clusters (see Figure 10) also share similarities with regard to the intensity, duration, or frequency of the CCX, supporting our choice of the primary clustering variable.

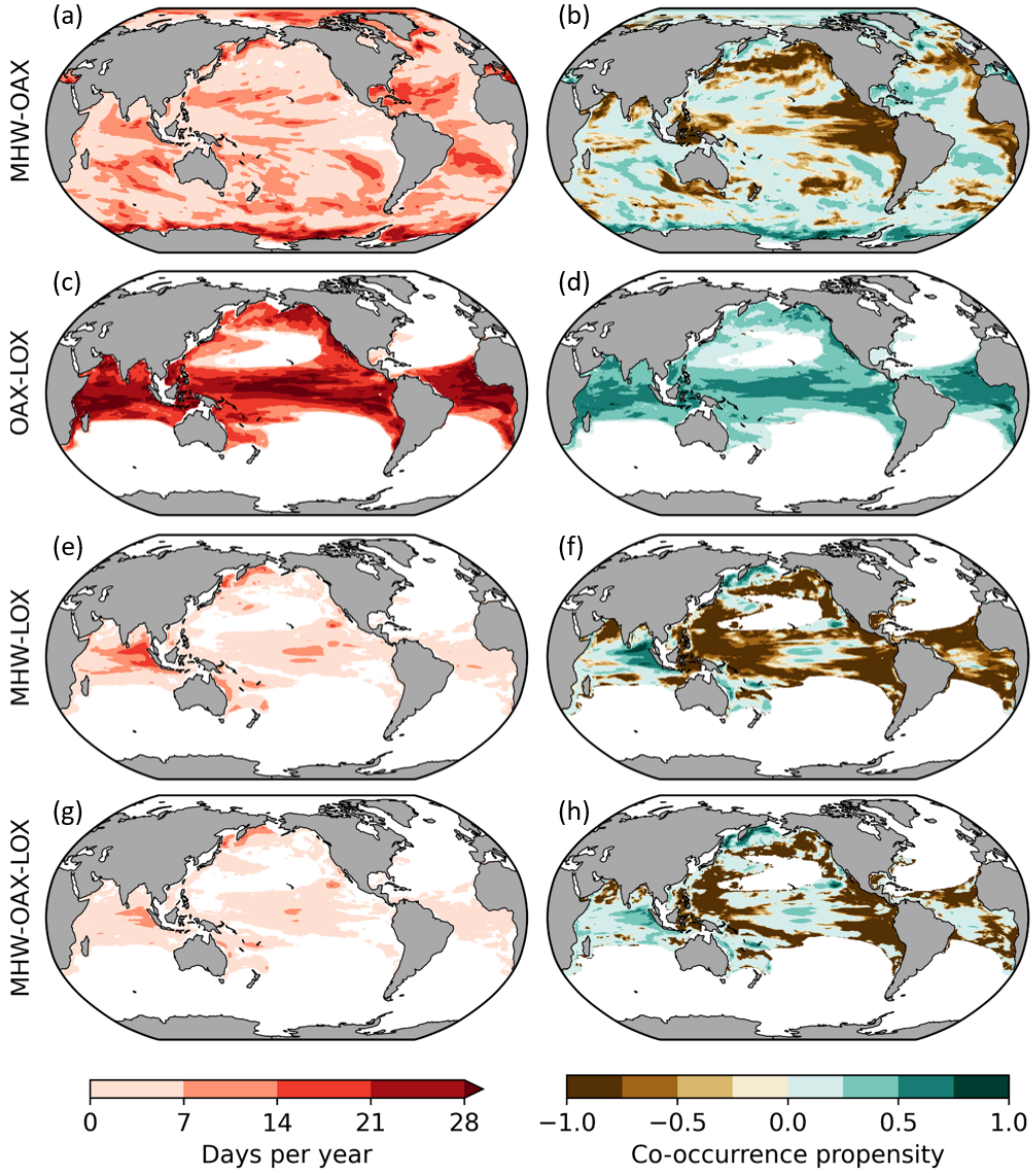


Figure 7. Spatial distribution of CCX illustrated by: CCX days per year (left column) and mean co-occurrence propensity of CCX (right column). The co-occurrence propensity represents the propensity of two column-single extremes occurring in the same column (Section 3.3). Each row corresponds to one CCX type, i.e. (a,b): MHW-OAX, (c,d): OAX-LOX, (e,f): MHW-LOX, (g,h): MHW-OAX-LOX.

574 The clustering for the MHW-OAX events results in four clusters (see Figure 10 left
 575 column). Clusters 2, 3, and 4 roughly correspond to the Subtropics, Subantarctic zone,
 576 and Antarctic zone. Cluster 1 covers the largest area by fraction (57.5%). However, it
 577 also has the shortest duration, lowest days per year, and lowest intensity index. On the
 578 contrary, cluster 4 is the highest in these metrics.

579 Across all clusters (even that of other CCX types), MHW-OAX clusters 1 and 2
 580 stand out as the only CCXs whose component extremes (MHW and OAX) are intensified
 581 simultaneously at the surface, occupying about 40 % of the water column on av-

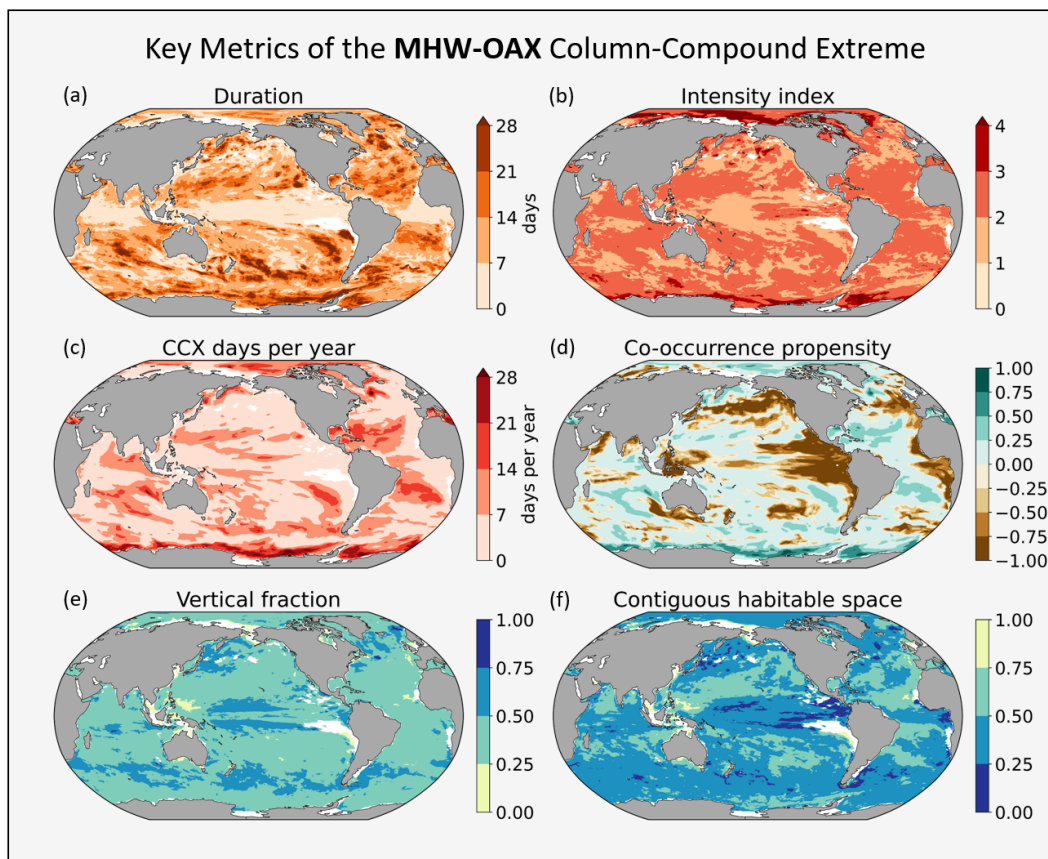


Figure 8. Key metrics of MHW-OAX events in the global ocean. (a) Mean duration, (b) mean annual maximum intensity index, (c) mean annual CCX days, (d) mean co-occurrence propensity, (e) mean fraction of water column occupied by extremes, and (f) mean fraction of contiguous habitable space in the vertical column

582 erage, and 81 % in area fraction of MHW-OAX events. In cluster 2, we see the strongest
 583 surface intensified signal, with MHW and OAX co-occurring at the same depths of 0 – 100 m.
 584 The co-occurrence of MHW and OAX in the tropics and subtropics near the surface sug-
 585 gests that OAX is primarily induced by MHW, and is elucidated by Burger et al. (2022);
 586 Burger and Frölicher (2023), who detected surface MHW-OAX events in the same re-
 587 gions. Increases in temperature during MHWs directly lead to an increase in $[H^+]$ through
 588 shifts in the carbonate chemistry equilibrium. MHWs on the surface also increases strat-
 589 ification and reduces the mixing of deep, nutrient-rich waters. Biological productivity
 590 is suppressed, leading to an increase in DIC and thus $[H^+]$. In cluster 1, we observe a
 591 bimodal depth distribution of the MHW and OAX signals, with one at the surface sim-
 592 ilar to cluster 2, and a weaker distribution in the subsurface. This cluster occurs on the
 593 borders of the other clusters and act as a transition zone between them, as waters are
 594 being mixed and advected. Surface waters extreme in MHW-OAX may be horizontally
 595 advected through ocean currents (Holbrook et al., 2019; Sen Gupta et al., 2020; Elza-
 596 haby et al., 2021). Furthermore, downwelling Kelvin and Rossby waves propagate, main-
 597 tain, and deepen the MHW-OAX signal (Holbrook et al., 2019; Zhang et al., 2021; Maul-
 598 ida et al., 2022; Qi et al., 2022). Surface and subsurface waters extreme with MHW and
 599 OAX may mix horizontally, forming the depth distribution seen in cluster 1.

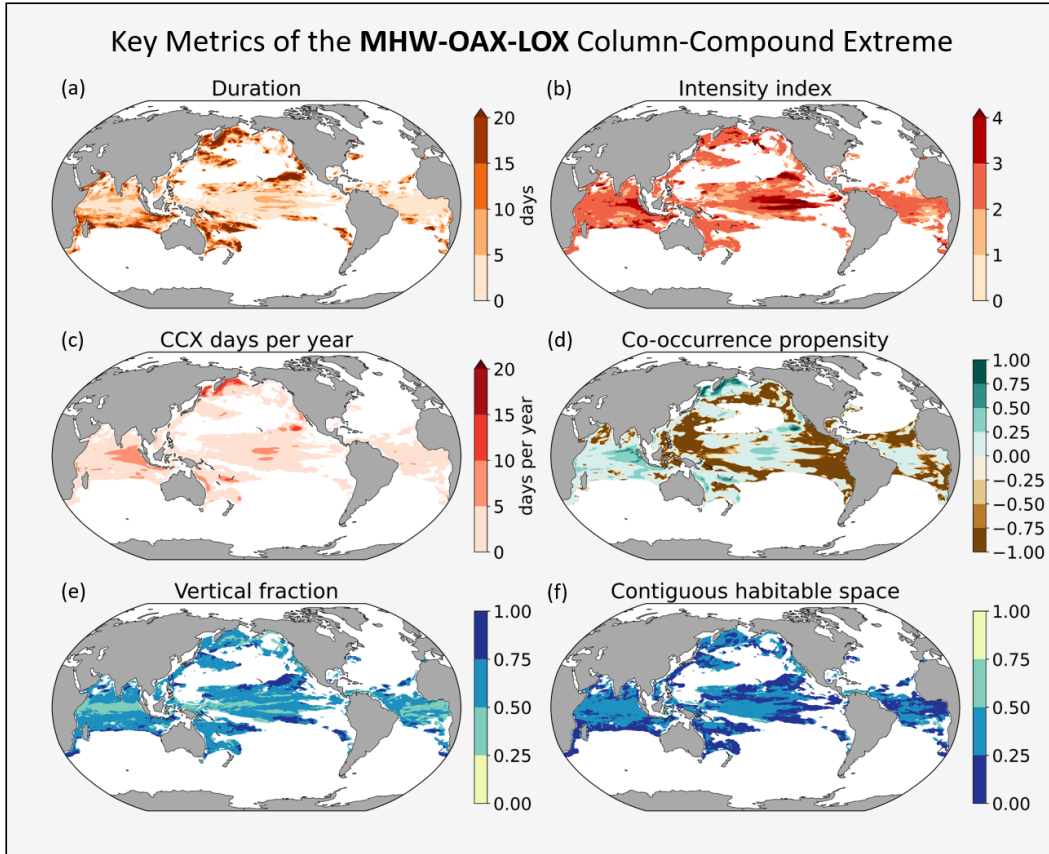


Figure 9. As Figure 8, but for triple compound events.

600 In clusters 3 and 4 we see the opposite, with MHW and OAX co-occurring in the
 601 subsurface. In cluster 3, we observe MHW intensified beneath the surface between 50–300 m,
 602 with OAX occurring in the lower half of the water column below 100 m. The spread across
 603 the water column causes this cluster to have the highest vertical fraction of 46%. Much
 604 of the cluster lies in the Subantarctic zone, within the Antarctic Circumpolar Current
 605 (ACC). In particular, the Scotia Sea, Drake Passage, and Macquarie Ridge stand out as
 606 regions with enhanced diapycnical mixing (Ledwell et al., 2011). Strong wind-driven cur-
 607 rents and rough bathymetry may mix surface MHWs into the subsurface (Pellichero et
 608 al., 2017; Vogt et al., 2022). Local parcels of water carrying the MHW signal may be dis-
 609 connected from the surface, and later reconnected again through mixing and surface heat-
 610 ing. Meanwhile, anomalous intensification of winds drive the upwelling of CO_2 -rich wa-
 611 ters within the ACC and Antarctic convergence zone (Negrete-García et al., 2019; Ra-
 612 madhan et al., 2022), heaving the thermocline and hence also waters with higher acid-
 613 ity, inducing OAX in the subsurface. The events of cluster 4 occur along the continent
 614 of Antarctica, with co-located MHW and OAX occurring largely beneath the surface be-
 615 tween 100–300 m. Here, MHW-OAX events have the highest frequency of 21 days per
 616 year, the longest mean duration of 19 days, and have the highest intensity index of 3.3.
 617 Strengthened zonal westerlies driving the Antarctic Circumpolar Current (ACC) could
 618 lead to increased upwelling of Circumpolar Deep Water (CDW) at the northern edge of
 619 the sea-ice zone (Morrison et al., 2015; Wilson et al., 2019; Ramadhan et al., 2022). This
 620 results in vertical entrainment of deep waters which tend to be warmer and more acidic
 621 (Gordon, 1981; Gordon & Huber, 1990; Pellichero et al., 2017). In periods of anomalously

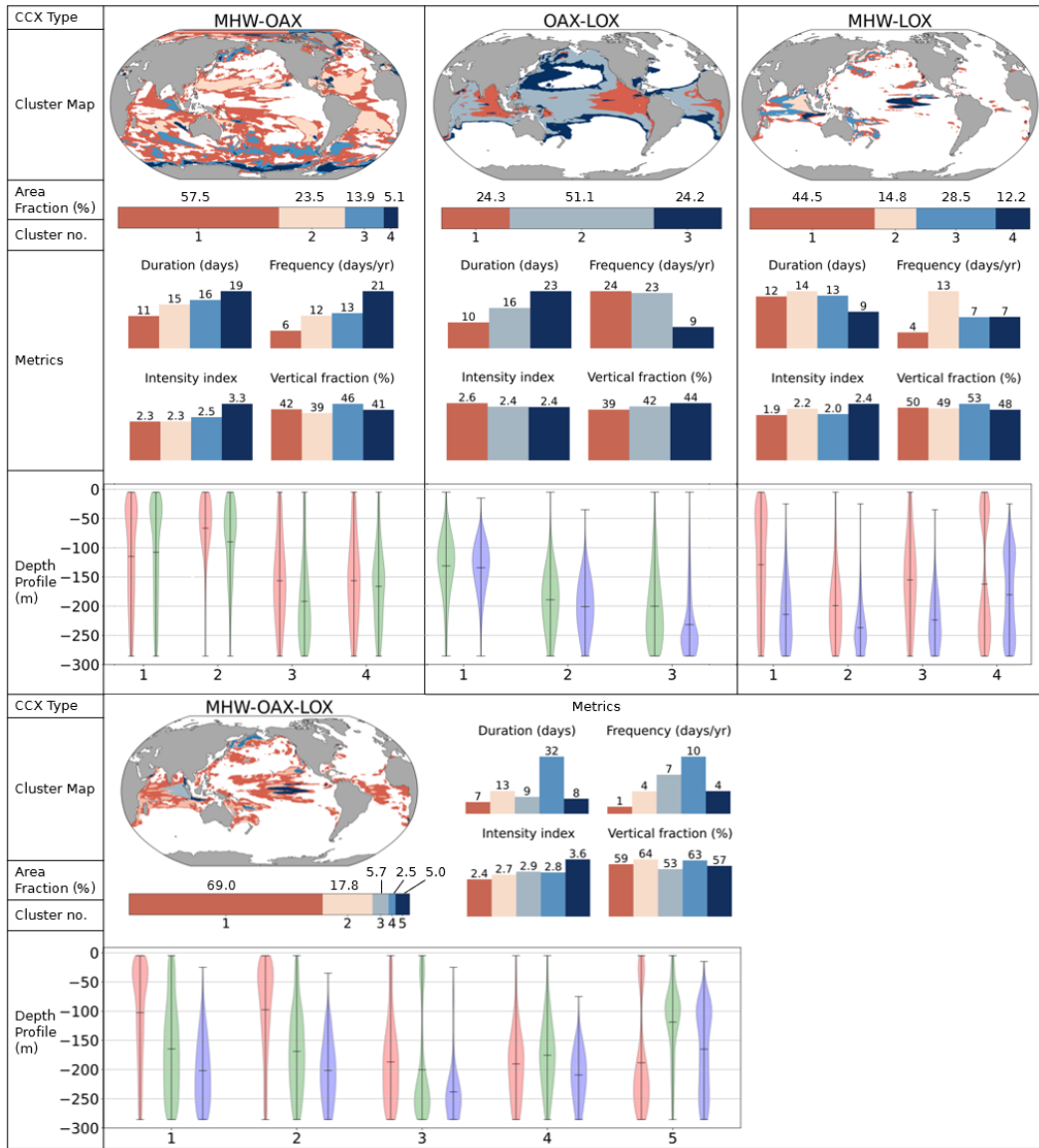


Figure 10. Summary of the main cluster characteristics identified by k-means clustering for each CCX type, i.e., MHW-LOX (top left column), OAX-LOX (top middle column), MHW-LOX (top right column), and the triple CCX MHW-OAX-LOX (bottom row). For each type, four groups of characteristics are provided (from the top): Horizontal distribution by a cluster map, cluster numbers and the area fraction occupied by each cluster as a horizontal bar plot, key metrics including cluster-averaged values of mean duration, mean days per year, mean annual column-maximum intensity index, and mean vertical fraction occupied by extremes as a vertical bar plots, and vertical distribution in the form of vertical violin plots. The latter show the sum of single grid-cell extreme occurrences during CCXs, weighted by their intensity index.

622
623

low sea ice extent, increased exposure of the surface to westerlies will also enhance upwelling of the CDW (Ramadhan et al., 2022).

624
625

OAX-LOX events are divided into three clusters (see Figure 10 middle column), where each cluster may be found in the same areas of each ocean basin. Cluster 1 roughly

626 corresponds to the eastern tropics and the Eastern Boundary Upwelling Systems (EBUS)
 627 regions, with OAX and LOX located together between 100 m and 300 m deep. Cluster
 628 2 events are located higher in the water column, between 50 m and 200 m, and are lo-
 629 cated along the boundaries of cluster 1, reaching to the western side of the basins. Clus-
 630 ter 3 is located along the boundaries of the subtropical gyres, where the deepest events
 631 are found at below 100 m. The locations and depths of these clusters are reflective of the
 632 locations of oxygen minimum zones (OMZs), which are closest to the surface in the EBUS,
 633 eastern tropical Pacific, subarctic Pacific, and the Indian Ocean, deeper in the western
 634 tropics, and disappears towards the subtropical gyres (Gilly et al., 2013). This suggests
 635 that OAX-LOX events are caused by variability in the size, intensity, and vertical posi-
 636 tion of OMZs. The association of low pH and low oxygen in waters at depth is also well-
 637 known (Paulmier et al., 2011; Gobler & Baumann, 2016), so that OMZ variability can
 638 be linked to OAX-LOX events. Upwelling regions like the EBUS and equatorial regions
 639 are susceptible to the shoaling of the OMZ by anomalous wind-driven upwelling/thermocline
 640 heaving events (Espinoza-Morriberón et al., 2019; José et al., 2019; Turi et al., 2018; Köhn
 641 et al., 2022). Deep waters high in carbon and low in oxygen are upwelled, which man-
 642 ifests as a OAX-LOX signal. Anomalous upwelling is also identified in the Gulf of Alaska,
 643 driven by variable wind stress curl and depressed sea surface height in the subpolar gyre
 644 (Hauri et al., 2021). In the western tropical Pacific and tropical Indian ocean, OAX-LOX
 645 events likely also occur during a shoaling of the thermocline, so that the OMZ shifts lat-
 646 erally closer to the surface (Xu et al., 2017; Leung, Thompson, et al., 2019; G. Yang et
 647 al., 2019).

648 Due to the high spatial correlation between MHW-LOX and MHW-OAX-LOX events,
 649 their clusters are also analogous (contrast Figure 10 right column with bottom row). MHW-
 650 OAX-LOX cluster 5 (MHW-LOX cluster 4) is located in the central equatorial Pacific,
 651 is the most intense (3.6) of all CCX clusters, but has a relatively short duration (9 days)
 652 and low days per year (4 days per year). The triple compound cluster with the longest
 653 duration (32 days) and highest days per year (10 days per year) is found in the Bering
 654 sea of cluster 4 (MHW-LOX cluster 2). In the eastern tropical Indian ocean, we find MHW-
 655 OAX-LOX cluster 3 (MHW-LOX cluster 2) occurring 7 days per year. Finally, MHW-
 656 OAX-LOX clusters 1 and 2 (MHW-LOX clusters 1 and 3) occupies the largest area frac-
 657 tion of 86.8%, and borders the other clusters in the tropics and North Pacific.

658 In MHW-OAX-LOX clusters 1 and 2, surface intensified extreme signals in tem-
 659 perature are clearly separated from the depth intensified signals in acidity and oxygen,
 660 as vertical entrainment and/or mixing is restricted across the thermocline. . Anomalous
 661 heating of the surface stratifies the surface layer and confines the MHW signal to the top
 662 100–150 m of the column. Meanwhile, OAX and LOX are intensified below the MHW
 663 during heaving or upwelling events. However, certain conditions allow heat to transfer
 664 below the thermocline leading to distinctive CCX depth profiles. The MHW-OAX-LOX
 665 cluster 5 in the central tropical Pacific is one such example, where MHW is intensified
 666 at the surface (0–50 m), and at depth (150–300 m). Meanwhile, OAX and LOX occu-
 667 pies the gap between 50–150 m. During El Niño periods, strong anomalous surface heat-
 668 ing takes place in the eastern tropical Pacific, deepening the thermocline and inducing
 669 MHWs throughout the water column (Fiedler & Lavín, 2017). On the western side of
 670 the Pacific the thermocline shoals, causing subsurface OAX and LOX extending into the
 671 central tropical Pacific (Xu et al., 2017; Leung, Thompson, et al., 2019). Thus the triple
 672 compound occurs when all three stressors occur in the same column, albeit at different
 673 vertical locations. When the surface heating tapers towards the end of El Niño, the MHW
 674 signal at the bottom of the column remains below the thermocline and is cut off from
 675 surface ventilation, leading to the characteristic depth profile seen in Figure 10. This sub-
 676 surface MHW signal persists even into the succeeding La Niña event, where the shoal-
 677 ing thermocline in the east leads to intensified OAX and LOX above the MHW. This
 678 process is illustrated in the Hovmoller schematic of Figure 12, and through a video (Sup-
 679 porting Information Movie S1).

680 In the eastern tropical Indian ocean and the Bering sea, corresponding to MHW-
 681 OAX-LOX clusters 3 and 4, an unusual combination of all three stressors co-occur in the
 682 subsurface below 100 m with little to no surface-MHW expression. Unlike the Antarc-
 683 tic region, there is not any known deep water mass of higher temperature in these ar-
 684 eas. One possible cause of MHW-OAX-LOX in cluster 4 is the Pacific Blob event in 2014-
 685 2016, which saw intense MHWs covering the northeastern Pacific, mixing into the sub-
 686 surface and persisting below the mixed layer. Triple compound events of MHW, OAX,
 687 and LOX were also found in the water column during this time (Gruber et al., 2021).
 688 The warm water mass advected into the Bering Sea in 2017-2018 (Basyuk & Zuenko, 2020;
 689 Stabeno & Bell, 2019), and may be represented by a peak in MHW-OAX-LOX in 2018
 690 (Supporting Information Figure S11). Subsequently, lower sea-ice cover in the winter led
 691 to anomalous stratification and reduced vertical mixing from melting ice (Stabeno & Bell,
 692 2019; Scannell et al., 2020), prolonging the lifetime of the CCX in the subsurface. In clus-
 693 ter 3, the largest event occurred in 1997, corresponding with the largest event of clus-
 694 ter 5, and a strong El Niño event (Supporting Information S11). This suggests an ENSO
 695 teleconnection in the Indian ocean leading to subsurface MHW-OAX-LOX. In these two
 696 clusters, few MHW studies have been done, and even less so on subsurface MHW, OAX,
 697 and LOX. As research in this space has been gradually gaining attention, we expect to
 698 better understand the mechanisms behind these subsurface triple compound events in
 699 the future.

700 4.5 Enhancement and Suppression of CCXs during ENSO Events

701 Further insights into the potential drivers of CCX can be deduced from when the
 702 CCX occur. We have already seen that at the global scale, most CCX tend to correlate
 703 positively with ENSO (Figure 6). But we also identified more complex responses with
 704 enhanced occurrences during both strong El Niños and strong La Niñas. Thus, it is well
 705 warranted to examine this connection in depth, looking at the regional changes in CCX
 706 days during El Niño (Figure 11a,c,e,g) and La Niña (Figure 11b,d,f,h) events.

707 During ENSO events, there is an enhancement of all MHW-related CCXs in the
 708 tropics across all basins, up to 10 days per year in many areas (Figures 11a-b,e-f,g-h).
 709 There are clear spatial differences between the opposite phases of ENSO for MHW-OAX
 710 (Figures 11a-b). In general, El Niño does not suppress MHW-OAX strongly in any lo-
 711 cation, but instead enhances it in the tropics and subtropics of all ocean basins by about
 712 20 days per year on average. There is particularly strong enhancement of up to 30 days
 713 per year in the Atlantic ocean and Arabian sea, which can be attributed to teleconnec-
 714 tions with ENSO (Holbrook et al., 2019; Sen Gupta et al., 2020; Chatterjee et al., 2022).
 715 During La Niña, surface MHW-OAX may be observed in the typical chevron pattern of
 716 the western subtropical Pacific (Holbrook et al., 2019). The regions highlighted belong
 717 to MHW-OAX clusters 1 and 2, both of which have a strong surface expression. There
 718 are also more distinct features across the globe during La Niña. Notably, there are con-
 719 fined regions of strong enhancement and suppression in the Subantarctic and Antarc-
 720 tic zones, and mostly fall within MHW-OAX clusters 3 and 4. These clusters have a stronger
 721 subsurface expression, but the same regions can be identified in Holbrook et al. (2019)
 722 linking surface MHW to various climate modes. In these regions, modes such as the south-
 723 ern annular mode (SAM) likely drive variability in surface wind stress, leading to changes
 724 in the depth of the thermocline and hence subsurface extremes.

725 With MHW-LOX and MHW-OAX-LOX, there are no distinct spatial differences
 726 between the positive and negative phases of ENSO, with the exception of the central equa-
 727 torial Pacific. Here, there is a strong increase in annual CCX days during El Niño by up
 728 to 30 days per year. This corresponds to cluster 5 of the triple compound event, which
 729 has most distinctive peak in volume fraction in the El Niño years of 1997 and 2016 (Sup-
 730 porting Information Figure S11). Both the surface MHW from the east and the subsur-
 731 face OAX and LOX from the west trace their driver to El Niño, thus having a single com-

mon driver, though operating through different processes in different sides of the tropical Pacific. The lack of a strong ENSO correlation in the eastern tropical Pacific is different from the results of Holbrook et al. (2019); Sen Gupta et al. (2020) where there is a strong response in the eastern equatorial Pacific. This was also reflected in the co-occurrence propensities of MHW-related CCXs (Figure 7. MHWs induced on the surface during El Niño strongly stratify the surface, suppressing the upwelling of deep waters and hence reducing the occurrence of OAX and LOX. While some surface MHWs induce co-located OAX, the variability of $[H^+]$ due to this temperature effect is lower than that of upwelled low carbon waters during other periods such as La Niña, and is hence not detected as extreme within the 95th percentile.

Among the CCX variations, OAX-LOX events stand out as having the most distinct ENSO associations 11c-d) in both spatial distribution and magnitude. In the tropical Pacific, the opposing effects of El Niño and La Niña phases are clear. During El Niño, OAX-LOX events are enhanced in the west by more than 30 days (cluster 2), representing a doubling in annual CCX days. Meanwhile, a strong suppression of up to 30 days is observed in the eastern tropical Pacific (cluster 1). Conversely during La Niña, the eastern tropical Pacific (cluster 1) experiences an enhancement of OAX-LOX of a similar magnitude, and a weaker suppression in the west (cluster 2). These events can be strongly linked to ENSO with the shoaling and deepening of the thermocline, as highlighted in the previous section. ENSO effects on OAX-LOX in other regions are also strong, though not as distinctly dichotomous between phases. They are typically facilitated by atmospheric teleconnections (Roy & Reason, 2001) and ocean currents (Susanto et al., 2001; Feng et al., 2018), through mechanisms such as thermocline and upwelling modulations.

5 Discussion

Most studies on marine extremes have focused so far on surface MHWs, permitting scientists to limit their analyses to the drivers and impacts occurring in the surface layer. With the CCXs detected in this study, there is a need to infer surface and subsurface drivers. Moreover, CCXs in this study with surface expressions extend at least 50 m into the subsurface, prompting an investigation of surface stratification and the mixed layer. Similarly, the associated impacts of CCXs are relevant not just to organisms residing at a certain depth, but also to those who inhabit the entire water column. These migrating organisms are impacted to a greater extent as CCXs shrink and divide their habitable space.

5.1 Drivers of Column-Compound Extreme Events

The most significant CCX clusters identified in Section 4 are summarised in Figure 12, with their corresponding metrics and vertical structure. Within these clusters, we find that CCXs tend to occur at similar depths, suggesting similar drivers. With the analysis we have also repeatedly identified ENSO events as the main driver of large proportion of CCXs. This is due to the large area of the Pacific ocean typically affected by ENSO, and the atmospheric and oceanic connections it has with other ocean basins. However, the mechanisms through which ENSO drives CCX varies with region. Furthermore, ENSO events can drive CCXs through multiple mechanisms.

Some of these ENSO-driven CCXs have been identified as being spatially co-occurring, where their constituent single extremes co-occur in the same grid cells and tend to driven by similar mechanisms. The most prominent example is OAX-LOX, which primarily occurs in the subsurface. The OAX-LOX clusters 1 and 2 exhibit this effect at different depths, which are dependent on the location of the thermocline. La Niña events associated with an increase in surface winds drive anomalous upwelling of low-pH and low-oxygen waters in California and Humboldt current systems, leading to events in the OAX-

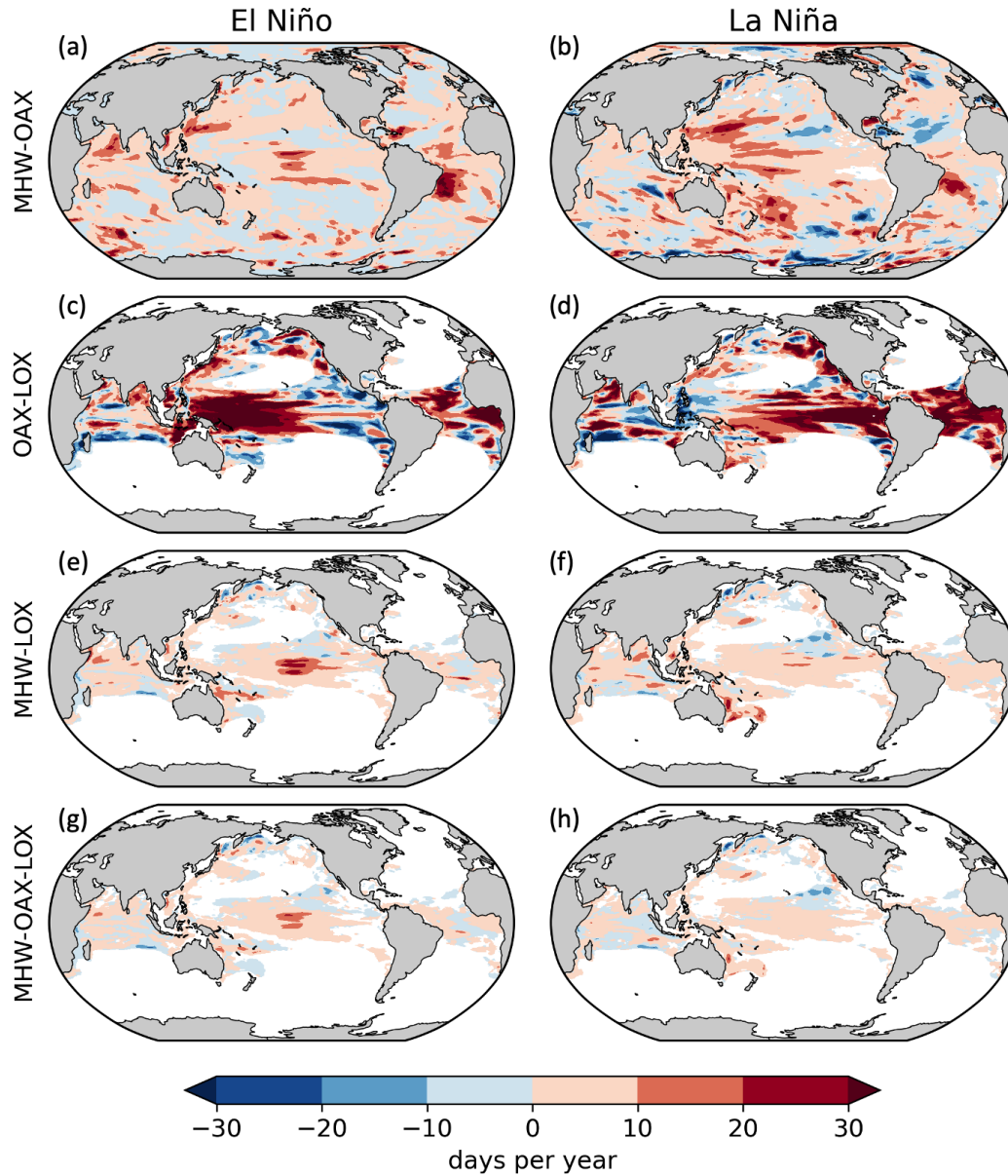


Figure 11. Maps illustrating the impact of ENSO on the number of extreme days for each CCX type. Shown are changes of annual CCX days during positive (left column) and negative (right column) ENSO phases, compared to a neutral ENSO phase. Each row corresponds to one CCX type, i.e. (a-b): MHW-OAX, (c-d): OAX-LOX, (e-f): MHW-LOX, (g-h): MHW-OAX-LOX. In this figure, a year is defined to begin in July and end in June of the next year, permitting to better capture the impact of ENSO as it peaks around Christmas.

782 LOX 1 cluster. Furthermore, the enhanced biological productivity induced by the up-
 783 welled waters further depletes oxygen through remineralisation. The depth of OAX and
 784 LOX during OAX-LOX events in the EBUS regions and east tropics cluster lies between
 785 50 – 200 m, which corroborates with the typical coastal and offshore upwelling source wa-
 786 ters of 150 – 280 m (Chhak & Di Lorenzo, 2007; Frischknecht et al., 2018; Bograd et al.,
 787 2015), and sits beneath the mean mixed layer depth (Ando & McPhaden, 1997; Fiedler

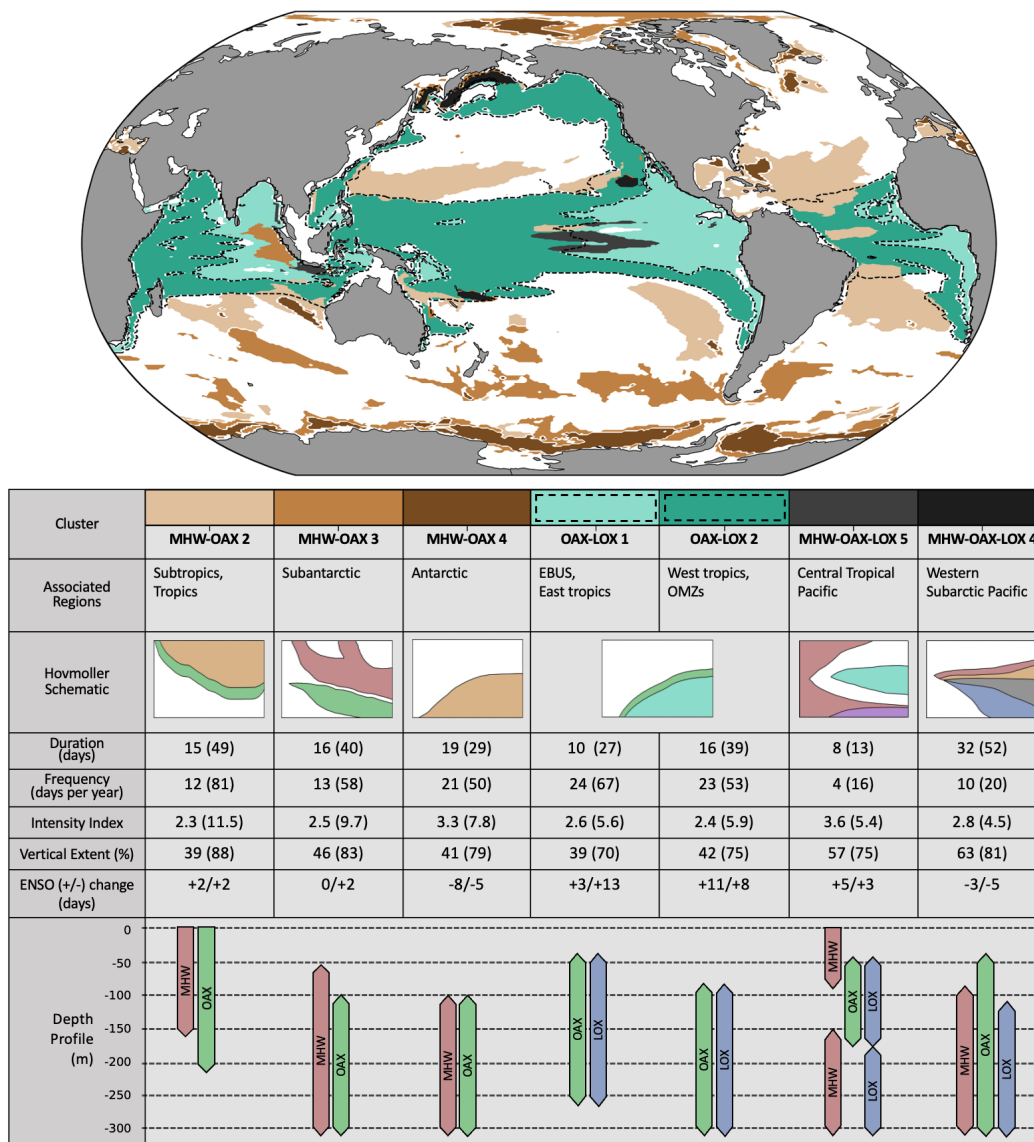


Figure 12. Synthesis figure of CCX properties in selected clusters. Map: Selected clusters of CCXs in a composite plot. The extent of OAX-LOX 1 and OAX-LOX 2 are marked by dashed lines to indicate their overlap with other clusters. Table (from top to bottom): Cluster names and their associated regions. Hovmoller schematics that are drawn to illustrate actual extreme conditions seen in the hindcast. Cluster mean values of mean duration, mean frequency, mean intensity index, mean vertical extent, and change in number of CCX days during positive and negative ENSO periods. Values in brackets are of the fixed baseline. Lastly, the approximate vertical locations of single extremes during CCXs are represented with simplified bars.

788 & Talley, 2006). Furthermore, the shoaling of the thermocline in the east tropics intensifies OAX and LOX in the subsurface. The co-occurrence propensity and vertical location of these events correspond roughly with the locations of low oxygen zones or shadow zones (Luyten et al., 1983; Paulmier & Ruiz-Pino, 2009), which are often associated with low pH (Paulmier et al., 2011). In the western tropical Pacific corresponding to OAX-LOX cluster 2, El Niño events lead to the shoaling of the thermocline, bringing low pH

789
790
791
792
793

794 and low oxygen waters closer to the surface, with mean depths corresponding to the mean
 795 mixed layer depth (Ando & McPhaden, 1997; Fiedler & Talley, 2006). In general, these
 796 events are deeper in the column than their eastern counterparts due to the deeper mixed
 797 layer depths in the western tropical Pacific. These events have the highest days per year
 798 among the identified clusters, increasing by the most during ENSO events. Another ex-
 799 ample of spatially co-occurring CCXs driven by ENSO is MHW-OAX cluster 2, predom-
 800 inantly in the subtropics. ENSO-driven temperature anomalies lead to MHWs (Holbrook
 801 et al., 2019), which then induces OAX through shifts in the carbonate chemistry equi-
 802 librium (Zeebe & Wolf-Gladrow, 2001; Burger et al., 2022).

803 ENSO events can also drive CCXs through multiple mechanisms, as seen in MHW-
 804 OAX-LOX cluster 5. MHW is induced throughout the column by strong surface heat-
 805 ing during El Niño in the eastern tropical Pacific. Meanwhile, El Niño also drives the
 806 shoaling of the thermocline in western tropical Pacific, inducing OAX and LOX in the
 807 subsurface. A deep MHW also persists in the subsurface even after being disconnected
 808 from the surface MHW. The resultant CCX is one which occupies the entire water col-
 809 umn, driven by El Niño through different mechanisms. The MHW-OAX-LOX cluster
 810 4 is another peculiar example, of which one occurrence in 2018 has been linked an El Niño
 811 event in 2014-2016 (Basyuk & Zuenko, 2020). Lateral advection of a warm water mass,
 812 enhanced southerly winds, and lower sea ice cover lead to the anomalous conditions in
 813 the Bering sea. The cluster has a low average association with ENSO, since our anal-
 814 ysis does not account for lag times.

815 The CCXs in the Southern Ocean (MHW-OAX clusters 3 and 4) could be driven
 816 by various climate modes. Within these clusters, strong sub-cluster enhancements and
 817 suppression have been found during ENSO events, especially La Niña. Due to the var-
 818 ied ENSO response within the clusters, the cluster-mean change in days per year due to
 819 ENSO is rather muted. These CCXs have been found to be driven by a combination of
 820 surface heating, strong winds causing diapycnal mixing (Ledwell et al., 2011; Tamsitt
 821 et al., 2017), anomalous sea-ice cover (Ramadhan et al., 2022; Gordon, 1981), and up-
 822 welling along the Antarctic divergence zone (Morrison et al., 2015; Wilson et al., 2019;
 823 Ramadhan et al., 2022). These mechanisms can be linked to climate modes such as ENSO,
 824 SAM, IOD, and others.

825 **5.2 Potential Impacts of Column-Compound Extreme Events**

826 In this study we have identified a majority of CCXs occurring in the tropics and
 827 subtropics. The tropical nature of many CCXs is of particular concern given the fact that
 828 these regions are the harbinger of the highest diversity across nearly all trophic levels,
 829 ranging from phytoplankton (Righetti et al., 2019), zooplankton (Benedetti et al., 2021),
 830 fish (Stuart-Smith et al., 2013), to top predators (Worm & Tittensor, 2018). Also, the
 831 frequent occurrence of very intense MHW-OAX events in the high latitude Southern Ocean
 832 hits a very sensitive ecosystem, with a relatively high diversity (Chown et al., 2015).

833 Compounded extreme events are able to cause severe impacts when the stressors
 834 interact synergistically (Gruber et al., 2021). This synergism can happen in different ways.
 835 The most direct effects occur when an organism experiences multiple stressors in the same
 836 place and time (Le Grix et al., 2021; Burger et al., 2022). In our study, we additionally
 837 consider the contraction of habitable space within the water column during CCXs, where
 838 extremes may be occurring at different depths. This contraction may lead to indirect im-
 839 pacts related to predator evasion or food availability.

840 Co-located, co-temporal events exacerbate impacts on organisms to which multi-
 841 ple stressors are synergistically detrimental, and is highly dependent on the species and
 842 life stage (Kroeker et al., 2013; Deutsch et al., 2015; Gobler & Baumann, 2016). Dur-
 843 ing compounded MHW and LOX, thermal stress increases metabolism and drives ad-
 844 ditional oxygen demand in ectotherms (Pörtner, 2002; K. E. Smith et al., 2023). The co-

845 inciding low oxygen environment further hinders the organisms' ability to survive, grow,
 846 or recruit. Recent works have quantified this effect into a composite "metabolic" or "aer-
 847 obic growth" index (Deutsch et al., 2015; Clarke et al., 2021). MHWs and LOX occur-
 848 ring in the same place and time will pose a large threat in this case, albeit shown to be
 849 relatively uncommon in this work. However, a strong MHW can simultaneously induce
 850 lower oxygen (due to lower solubility), and reduce the low oxygen tolerance threshold
 851 of the organism (through increased metabolism), effectively increasing the oxygen thresh-
 852 old beyond those used in this study. Furthermore, acidic conditions have been shown to
 853 increase metabolic stress (Pan et al., 2015; Engström-Öst et al., 2019; Tai et al., 2021;
 854 Lattuca et al., 2023). Thus the co-occurrence of OAX adds another layer of metabolic
 855 demand. Every organism has a different metabolic threshold (Deutsch et al., 2015), and
 856 it is beyond the range of this study to identify impacts on any particular species. How-
 857 ever, higher resolution regional studies (Franco et al., 2022) in conjunction with labo-
 858 ratory studies (Seibel et al., 2016) will be able to identify the impacts on metabolism of
 859 any given species.

860 Up until now, there is very little work on the compression of marine habitats due
 861 to extreme events (Desmet et al., 2022; Köhn et al., 2022), and much less so with com-
 862 pounded extreme stressors. In this study we show that when CCXs occur, the remain-
 863 ing continuous habitable space is less than half of the water column on average. This frac-
 864 tion reduces further when multiple extremes occur in different parts of the water column.
 865 Vertically migrating organisms are expected to be especially impacted by CCXs, since
 866 they depend on the habitable water column for essential biological activities. Diel ver-
 867 tical migration (DVM) is understood to be performed by planktonic species for the pur-
 868 pose of food gathering and predator avoidance (Ritz et al., 2011), and is a behavioural
 869 response to light (Cohen & Forward, 2019). Little is known about the impact of marine
 870 extremes on DVM, except that some species regularly migrate into low oxygen and low
 871 pH environments (Riquelme-Bugueño et al., 2020). When extreme conditions occurs close
 872 to the surface, the habitable space of migrating organisms is reduced. They may avoid
 873 the extreme conditions on the surface, thereby reducing food availability, or simply con-
 874 tinue to migrate upwards into extreme conditions, increasing metabolism and food dem-
 875 and. In either case, ability of the organisms to grow and survive is reduced. In the event
 876 of a CCX that covers both the surface and subsurface, the migrating organisms have no
 877 good choice to make, and are simply subject to extreme conditions where ever they are.
 878 Habitat contraction may further impact organisms in more indirect ways. Extreme con-
 879 ditions on the surface may force marine fish to migrate into the subsurface (Jorda et al.,
 880 2020), decreasing the survivability of zooplankton species which use the darker environ-
 881 ment to avoid predators.

882 **5.3 Caveats and Limitations**

883 Owing to the lack of data, the model results were evaluated with respect to sur-
 884 face MHWs and OAXs only, leaving us largely blind with regard to potential biases of
 885 the important processes at depth causing CCX. The evaluation of the surface OAX with
 886 OceanSODA-ETHZ (Gregor & Gruber, 2021) showed a tendency of the model towards
 887 longer and more intense events on the surface. Since this bias is located in the upwelling
 888 regions, we also expect it to apply to detected LOXs, due to their high co-occurrence in
 889 these regions. Overall, we expect the impact of potential biases on our results to be re-
 890 stricted to particular metrics, perhaps most importantly the intensity and duration of
 891 the events. In contrast, the spatial structure of the CCX and their co-occurrence propen-
 892 sity is likely much less affected, as this is a result of large-scale processes, which we con-
 893 sider well captured by the model. One option for the subsurface evaluation of these prop-
 894 erties is emerging from the rapidly increasing number of observations from the Biogeo-
 895 chemical Argo float program (Johnson & Claustre, 2016). These observations could be
 896 used to evaluate $[H^+]$ and $[O_2]$ in the subsurface, though their 10 day repeat cycle and
 897 wide spacing will require quite some effort to arrive at a robust extreme product.

898 A second caveat concerns the relatively low resolution of the atmospheric forcing
 899 employed in our CESM hindcast. This low resolution of the forcing affects atmosphere-
 900 forced extreme events, while ocean-forced events are likely much less affected. In the case
 901 of the former, long duration events, such as those associated with ENSO, are better rep-
 902 resented compared to short duration events. In the case of ocean-forced events, e.g., through
 903 heaving and shoaling of the thermocline, we expect little impact of our choice. But still,
 904 and especially also when considering the moderate resolution of our model, our results
 905 are biased toward the longer-lasting CCXs extending over of substantial spatial scales.

906 The third caveat concerns the choice of criteria used to identify extremes. Our choices
 907 were made with the intention to investigate the co-occurrence of multiple stressors within
 908 the vertical column in a systematic and consistent manner, linking them to drivers and
 909 mechanisms based on their spatiotemporal characteristics. For this work, the moving base-
 910 line was primarily used, since it a better choice in the investigation of drivers behind ex-
 911 treme events. However in Figures 5 and 6 it was shown that the detected volume frac-
 912 tion is vastly different between that of the fixed and moving baselines. The results on
 913 the moving baseline are unable to show the worsening conditions of global ocean under
 914 climate change, nor the change in propensity of extreme events under such conditions.
 915 For such an analysis, the fixed baseline may be a better choice.

916 Furthermore, the chosen extreme criteria are not targeted towards specific biolog-
 917 ical thresholds or marine organisms. Thus, the impacts of the extremes identified in this
 918 study cannot be directly quantified. For example, MHW-OAX CCXs are generally ab-
 919 sent in the EBUS, even though temperature-induced OAXs are known to occur during
 920 MHWs. This is likely because the OAX occurrences in these regions are dominated by
 921 anomalous upwelling events, which reduce pH more strongly compared to MHWs. Thus
 922 we see more OAX-LOX occurring in the EBUS. However, this does not mean that the
 923 MHW-induced low pH is irrelevant, as there may be organisms still affected. In such sce-
 924 narios it is better to rely on species-specific thresholds as the basis of extreme detection.
 925 This limitation on biological impacts also extends to the definition of CCXs, where at
 926 least 50 m of each extreme type is required. An organism whose metabolism is affected
 927 by temperature could be affected by either MHWs or LOXs, and not necessarily only
 928 when both occur. It may then be a better choice to define extreme conditions based on
 929 the metabolic rate of the particular organism and oxygen concentration in the water.

930 6 Summary and Conclusions

931 With this work on CCX, we make the first step in characterising extremes that are
 932 compounded in the vertical water column. CCXs are detected in the global ocean on a
 933 CESM-BEC daily hindcast from 1961 to 2020. Key characteristics like frequency, du-
 934 ration, intensity, and reduction of habitable space are assessed, to determine the regions
 935 where CCXs are the most severe. These are the subtropics and Southern ocean for MHW-
 936 OAX, and the tropics and north Pacific for OAX-LOX, MHW-LOX, and MHW-OAX-
 937 LOX. All CCX substantially increase in their intensity, frequency, and spatial extent, pri-
 938 marily driven by ocean warming and the increase in the ocean's acidity owing to the oceanic
 939 uptake of anthropogenic CO₂ from the atmosphere.

940 Within the vertical column, the depths where single extremes occur during CCXs
 941 are analysed to determine the mechanisms behind them. We find that ENSO-associated
 942 CCXs tend to be driven by a single mechanism such as increased air-sea heat flux or in-
 943 creased upwelling, resulting in co-located compounded events. On the other hand, there
 944 is a significant proportion of CCXs where the constituent single extremes occur in dif-
 945 ferent parts of the vertical column. These tend to be driven by separate drivers, and have
 946 a reduced association with ENSO events.

947 Marine extreme events can have a large impact on pelagic organisms, which are usu-
948 ally affected by multiple, rather than a single stressor. These organisms swim or migrate
949 vertically, experiencing various physical and chemical conditions. The study of vertically
950 compounded extremes thus advances our understanding of the impacts of extreme events
951 on marine organisms. Furthermore, these extremes are likely to become more frequent
952 and intense with the climate trend of increasing temperatures and atmospheric CO₂. Ex-
953 treme conditions of the past may well become the mean state of the ocean in the future.
954 Further analysis of such column-compound events in regional scales or to with regard
955 to specific organisms will extend our understanding of their future impacts.

956 **Open Research**

957 All data to reproduce the plots can be found under the following repository: [https://](https://doi.org/10.3929/ethz-b-000626173)
958 doi.org/10.3929/ethz-b-000626173. Model output data may be obtained upon re-
959 quest from the corresponding author (joel.wong@usys.ethz.ch).

960 **Conflict of Interest Statement**

961 The authors have no conflicts of interest to declare.

962 **Acknowledgments**

963 This project has received funding from the European Union's Horizon 2020 research and
964 innovation programme under grant agreement No 820989 (COMFORT). The authors thank
965 Dr. Damian Loher for his modeling support, and Dr. Eike Köhn, Dr. Luke Gregor, and
966 Dr. Fabio Benedetti for useful discussions.

References

967

968

969

970

971

972

973

974

975

976

977

978

979

980

981

982

983

984

985

986

987

988

989

990

991

992

993

994

995

996

997

998

999

1000

1001

1002

1003

1004

1005

1006

1007

1008

1009

1010

1011

1012

1013

1014

1015

1016

1017

1018

1019

1020

- Ando, K., & McPhaden, M. J. (1997). Variability of surface layer hydrography in the tropical Pacific Ocean. *Journal of Geophysical Research: Oceans*, *102*(C10), 23063–23078. doi: 10.1029/97JC01443
- Basyuk, E., & Zuenko, Y. (2020). Extreme oceanographic conditions in the northwestern Bering Sea in 2017–2018. *Deep-Sea Research Part II: Topical Studies in Oceanography*, *181–182*. doi: 10.1016/j.dsr2.2020.104909
- Bednaršek, N., Feely, R. A., Beck, M. W., Glippa, O., Kanerva, M., & Engström-Öst, J. (2018). El Niño-related thermal stress coupled with upwelling-related ocean acidification negatively impacts cellular to population-level responses in pteropods along the California current system with implications for increased bioenergetic costs. *Frontiers in Marine Science*, *5*, 1–17. doi: 10.3389/fmars.2018.00486
- Benedetti, F., Vogt, M., Elizondo, U. H., Righetti, D., Zimmermann, N. E., & Gruber, N. (2021). Major restructuring of marine plankton assemblages under global warming. *Nature Communications*, *12*(1), 5226. doi: 10.1038/s41467-021-25385-x
- Bertrand, A., Ballón, M., & Chaigneau, A. (2010). Acoustic observation of living organisms reveals the upper limit of the oxygen minimum zone. *PLoS ONE*, *5*(4). doi: 10.1371/journal.pone.0010330
- Bianchi, D., & Mislán, K. A. (2016). Global patterns of diel vertical migration times and velocities from acoustic data. *Limnology and Oceanography*, *61*(1), 353–364. doi: 10.1002/lno.10219
- Bianchi, D., Stock, C., Galbraith, E. D., & Sarmiento, J. L. (2013). Diel vertical migration: Ecological controls and impacts on the biological pump in a one-dimensional ocean model. *Global Biogeochemical Cycles*, *27*(2), 478–491. doi: 10.1002/gbc.20031
- Bograd, S. J., Buil, M. P., Lorenzo, E. D., Castro, C. G., Schroeder, I. D., Goericke, R., . . . Whitney, F. A. (2015). Changes in source waters to the Southern California Bight. *Deep-Sea Research Part II: Topical Studies in Oceanography*, *112*, 42–52. doi: 10.1016/j.dsr2.2014.04.009
- Boyd, P. W., & Brown, C. J. (2015). Modes of interactions between environmental drivers and marine biota. *Frontiers in Marine Science*, *2*, 1–7. doi: 10.3389/fmars.2015.00009
- Braun, C. D., Kaplan, M. B., Horodysky, A. Z., & Llopiz, J. K. (2015). Satellite telemetry reveals physical processes driving billfish behavior. *Animal Biotelemetry*, *3*(1). doi: 10.1186/s40317-014-0020-9
- Burger, F. A., & Frölicher, T. L. (2023). Drivers of Surface Ocean Acidity Extremes in an Earth System Model. *Global Biogeochemical Cycles*, *37*(9), e2023GB007785. (Burger2023) doi: 10.1029/2023GB007785
- Burger, F. A., John, J. G., & Frölicher, T. L. (2020). Increase in ocean acidity variability and extremes under increasing atmospheric CO₂. *Biogeosciences*, *17*(18), 4633–4662. doi: 10.5194/bg-17-4633-2020
- Burger, F. A., Terhaar, J., & Frölicher, T. L. (2022). Compound marine heatwaves and ocean acidity extremes. *Nature Communications*, 1–12. doi: 10.1038/s41467-022-32120-7
- Chan, F., Barth, J. A., Lubchenco, J., Kirincich, A., Weeks, H., Peterson, W. T., & Menge, B. A. (2008). Emergence of anoxia in the California current large marine ecosystem. *Science*, *319*(5865), 920. doi: 10.1126/science.1149016
- Chatterjee, A., Anil, G., & Shenoy, L. R. (2022). Marine heatwaves in the Arabian Sea. *Ocean Science*, *18*(3), 639–657. doi: 10.5194/os-18-639-2022
- Chhak, K., & Di Lorenzo, E. (2007). Decadal variations in the California Current upwelling cells. *Geophysical Research Letters*, *34*(14), 1–6. doi: 10.1029/2007GL030203

- 1021 Chiswell, S. M. (2022). Global Trends in Marine Heatwaves and Cold Spells: The
 1022 Impacts of Fixed Versus Changing Baselines. *Journal of Geophysical Research:*
 1023 *Oceans*, 127(10), e2022JC018757. doi: 10.1029/2022JC018757
- 1024 Chown, S. L., Clarke, A., Fraser, C. I., Cary, S. C., Moon, K. L., & McGeoch, M. A.
 1025 (2015). The changing form of Antarctic biodiversity. *Nature*, 522(7557),
 1026 431–438. doi: 10.1038/nature14505
- 1027 Clarke, T. M., Wabnitz, C. C., Striegel, S., Frölicher, T. L., Reygondeau, G., & Che-
 1028 ung, W. W. (2021). Aerobic growth index (AGI): An index to understand
 1029 the impacts of ocean warming and deoxygenation on global marine fisheries
 1030 resources. *Progress in Oceanography*, 195. doi: 10.1016/j.pocean.2021.102588
- 1031 Cohen, J. H., & Forward, R. B. (2019). Vertical Migration of Aquatic Animals.
 1032 In J. C. Choe (Ed.), *Encyclopedia of Animal Behavior (Second Edition)* (pp.
 1033 546–552). Oxford: Academic Press. doi: 10.1016/B978-0-12-809633-8.01257-7
- 1034 Collins, M., Sutherland, M., Bouwer, L., Cheong, S.-M., Frölicher, T., Des Combes,
 1035 H. J., ... Tibig, L. (2019). *Extremes, Abrupt Changes and Managing Risks*
 1036 (Tech. Rep.).
- 1037 Crain, C. M., Kroeker, K., & Halpern, B. S. (2008). Interactive and cumulative ef-
 1038 fects of multiple human stressors in marine systems. *Ecology Letters*, 11(12),
 1039 1304–1315. doi: 10.1111/j.1461-0248.2008.01253.x
- 1040 Desmet, F., Gruber, N., Köhn, E. E., Münnich, M., & Vogt, M. (2022). Tracking the
 1041 space-time evolution of ocean acidification extremes in the California Current
 1042 System and Northeast Pacific. *Journal of Geophysical Research: Oceans*, 1–30.
 1043 doi: 10.1029/2021jc018159
- 1044 Desmet, F., Münnich, M., & Gruber, N. (2023). *Spatiotemporal heterogeneity in*
 1045 *the increase of ocean acidity extremes in the Northeast Pacific*. doi: 10.5194/bg
 1046 -2023-60
- 1047 Deutsch, C., Ferrel, A., Seibel, B., Pörtner, H.-O., & Huey, R. B. (2015). Climate
 1048 change tightens a metabolic constraint on marine habitats. *Science*, 348(6239),
 1049 1132–1136. doi: DOI:10.1126/science.aaa1605
- 1050 Diaz, R. J., & Rosenberg, R. (2008). Spreading Dead Zones and Consequences
 1051 for Marine Ecosystems. *Science*, 321(5891), 926–929. doi: 10.1126/science
 1052 .1156401
- 1053 Di Lorenzo, E., & Mantua, N. (2016). Multi-year persistence of the 2014/15 North
 1054 Pacific marine heatwave. *Nature Climate Change*, 6(11), 1042–1047. doi: 10
 1055 .1038/nclimate3082
- 1056 Ebita, A., Kobayashi, S., Ota, Y., Moriya, M., Kumabe, R., Onogi, K., ... Ishimizu,
 1057 T. (2011). The Japanese 55-year Reanalysis “JRA-55”: An Interim Report.
 1058 *Sola*, 7, 149–152. doi: 10.2151/sola.2011-038
- 1059 Elzahaby, Y., Schaeffer, A., Roughan, M., & Delaux, S. (2021). Oceanic Circula-
 1060 tion Drives the Deepest and Longest Marine Heatwaves in the East Australian
 1061 Current System. *Geophysical Research Letters*, 48(17), e2021GL094785. doi:
 1062 10.1029/2021GL094785
- 1063 Engström-Öst, J., Glippa, O., Feely, R. A., Kanerva, M., Keister, J. E., Alin, S. R.,
 1064 ... Bednaršek, N. (2019). Eco-physiological responses of copepods and
 1065 pteropods to ocean warming and acidification. *Scientific Reports*, 9(1), 1–
 1066 13. doi: 10.1038/s41598-019-41213-1
- 1067 Espinoza-Morriberón, D., Echevin, V., Colas, F., Tam, J., Gutierrez, D., Graco,
 1068 M., ... Quispe-Calluari, C. (2019). Oxygen variability during ENSO in the
 1069 Tropical South Eastern Pacific. *Frontiers in Marine Science*, 5, 1–20. doi:
 1070 10.3389/fmars.2018.00526
- 1071 Feng, M., Zhang, N., Liu, Q., & Wijffels, S. (2018). The Indonesian throughflow, its
 1072 variability and centennial change. *Geoscience Letters*, 5(1), 3. doi: 10.1186/
 1073 s40562-018-0102-2
- 1074 Fiedler, P. C., & Lavín, M. F. (2017). Oceanographic Conditions of the Eastern
 1075 Tropical Pacific. In P. W. Glynn, D. P. Manzello, & I. C. Enochs (Eds.),

- 1076 *Coral Reefs of the Eastern Tropical Pacific: Persistence and Loss in a Dy-*
 1077 *namic Environment* (pp. 59–83). Dordrecht: Springer Netherlands. doi:
 1078 10.1007/978-94-017-7499-4_3
- 1079 Fiedler, P. C., & Talley, L. D. (2006). Hydrography of the eastern tropical Pacific:
 1080 A review. *Progress in Oceanography*, 69(2-4), 143–180. doi: 10.1016/j.pocean
 1081 .2006.03.008
- 1082 Fragkopoulou, E., Sen Gupta, A., Costello, M. J., Wernberg, T., Araújo, M. B.,
 1083 Serrão, E. A., ... Assis, J. (2023, September). Marine biodiversity exposed to
 1084 prolonged and intense subsurface heatwaves. *Nature Climate Change*, 1–8. doi:
 1085 10.1038/s41558-023-01790-6
- 1086 Franco, A. C., Kim, H., Frenzel, H., Deutsch, C., Ianson, D., Sumaila, U. R., &
 1087 Tortell, P. D. (2022). Impact of warming and deoxygenation on the habitat
 1088 distribution of Pacific halibut in the Northeast Pacific. *Fisheries Oceanogra-*
 1089 *phy*, 31(6), 601–614. doi: 10.1111/fog.12610
- 1090 Friedlingstein, P., Jones, M. W., Sullivan, M. O., Andrew, R. M., Bakker, D. C. E.,
 1091 Hauck, J., ... Peters, W. (2022). Global Carbon Budget 2021. *Earth System*
 1092 *Science Data*, 1917–2005. doi: 10.5194/essd-14-4811-2022
- 1093 Frischknecht, M., Münnich, M., & Gruber, N. (2018). Origin, Transformation,
 1094 and Fate: The Three-Dimensional Biological Pump in the California Current
 1095 System. *Journal of Geophysical Research: Oceans*, 123(11), 7939–7962. doi:
 1096 10.1029/2018JC013934
- 1097 Frölicher, T. L., Fischer, E. M., & Gruber, N. (2018). Marine heatwaves under
 1098 global warming. *Nature*, 560(7718), 360–364. doi: 10.1038/s41586-018-0383-9
- 1099 Gent, P. R., Danabasoglu, G., Donner, L. J., Holland, M. M., Hunke, E. C., Jayne,
 1100 S. R., ... Zhang, M. (2011). The Community Climate System Model Version
 1101 4. *Journal of Climate*, 24(19), 4973–4991. doi: 10.1175/2011JCLI4083.1
- 1102 Gilly, W. F., Michael Beman, J., Litvin, S. Y., & Robison, B. H. (2013). Oceano-
 1103 graphic and biological effects of shoaling of the oxygen minimum zone. *Annual*
 1104 *Review of Marine Science*, 5, 393–420. doi: 10.1146/annurev-marine-120710
 1105 -100849
- 1106 Gleckler, P. J., Durack, P. J., Stouffer, R. J., Johnson, G. C., & Forest, C. E.
 1107 (2016). Industrial-era global ocean heat uptake doubles in recent decades.
 1108 *Nature Climate Change*, 6(4), 394–398. doi: 10.1038/nclimate2915
- 1109 Gobler, C. J., & Baumann, H. (2016). Hypoxia and acidification in ocean ecosys-
 1110 tems: Coupled dynamics and effects on marine life. *Biology Letters*, 12(5). doi:
 1111 10.1098/rsbl.2015.0976
- 1112 Good, S., Embury, O., Bulgin, C., & Mittaz, J. (2019). *ESA Sea Surface Tem-*
 1113 *perature Climate Change Initiative (SST_cci): Level 4 Analysis Climate Data*
 1114 *Record, version 2.0*. Centre for Environmental Data Analysis (CEDA). doi:
 1115 10.5285/ACED40D7CB964F23A0FD3E85772F2D48
- 1116 Good, S., Fiedler, E., Mao, C., Martin, M. J., Maycock, A., Reid, R., ... Worsfold,
 1117 M. (2020). The Current Configuration of the OSTIA System for Operational
 1118 Production of Foundation Sea Surface Temperature and Ice Concentration
 1119 Analyses. *Remote Sensing*, 12(4), 720. doi: 10.3390/rs12040720
- 1120 Gordon, A. L. (1981). Seasonality of Southern Ocean Sea Ice. *Journal of Geophysi-*
 1121 *cal Research*, 86(C5), 4193–4197. doi: 10.1029/JC086iC05p04193
- 1122 Gordon, A. L., & Huber, B. A. (1990). Southern ocean winter mixed layer. *Journal*
 1123 *of Geophysical Research*, 95(C7), 11655. doi: 10.1029/jc095ic07p11655
- 1124 Gregor, L., & Gruber, N. (2021). OceanSODA-ETHZ: A global gridded data
 1125 set of the surface ocean carbonate system for seasonal to decadal studies
 1126 of ocean acidification. *Earth System Science Data*, 13(2), 777–808. doi:
 1127 10.5194/essd-13-777-2021
- 1128 Gruber, N., Boyd, P. W., Frölicher, T. L., & Vogt, M. (2021). Ocean Biogeochemical
 1129 Extremes and Compound Events. *Nature*, 600, 395–407. doi: 10.1038/s41586
 1130 -021-03981-7

- 1131 Hauck, J., Zeising, M., Le Quéré, C., Gruber, N., Bakker, D. C. E., Bopp, L., ...
 1132 Séférian, R. (2020). Consistency and Challenges in the Ocean Carbon Sink
 1133 Estimate for the Global Carbon Budget. *Frontiers in Marine Science*, 7.
- 1134 Hauri, C., Gruber, N., McDonnell, A. M., & Vogt, M. (2013). The intensity, du-
 1135 ration, and severity of low aragonite saturation state events on the California
 1136 continental shelf. *Geophysical Research Letters*, 40(13), 3424–3428. doi:
 1137 10.1002/grl.50618
- 1138 Hauri, C., Pagès, R., McDonnell, A. M., Stuecker, M. F., Danielson, S. L., Hed-
 1139 strom, K., ... Doney, S. C. (2021). Modulation of ocean acidification by
 1140 decadal climate variability in the Gulf of Alaska. *Communications Earth
 1141 and Environment*, 2(1), 1–7. Retrieved from [http://dx.doi.org/10.1038/
 1142 s43247-021-00254-z](http://dx.doi.org/10.1038/s43247-021-00254-z) doi: 10.1038/s43247-021-00254-z
- 1143 Hobday, A. J., Alexander, L. V., Perkins, S. E., Smale, D. A., Straub, S. C.,
 1144 Oliver, E. C., ... Wernberg, T. (2016). A hierarchical approach to defin-
 1145 ing marine heatwaves. *Progress in Oceanography*, 141, 227–238. doi:
 1146 10.1016/j.pocean.2015.12.014
- 1147 Hobday, A. J., Oliver, E. C., Gupta, A. S., Benthuisen, J. A., Burrows, M. T.,
 1148 Donat, M. G., ... Smale, D. A. (2018). Categorizing and naming marine
 1149 heatwaves. *Oceanography*, 31(2), 162–173. doi: 10.5670/oceanog.2018.205
- 1150 Hofmann, A. F., Peltzer, E. T., Walz, P. M., & Brewer, P. G. (2011). Hypoxia by
 1151 degrees: Establishing definitions for a changing ocean. *Deep-Sea Research Part
 1152 I: Oceanographic Research Papers*, 58(12), 1212–1226. doi: 10.1016/j.dsr.2011
 1153 .09.004
- 1154 Holbrook, N. J., Claar, D. C., Hobday, A. J., McInnes, K. L., Oliver, E. C. J.,
 1155 Gupta, A. S., ... Zhang, X. (2020). ENSO-Driven Ocean Extremes and Their
 1156 Ecosystem Impacts. *El Niño Southern Oscillation in a Changing Climate*,
 1157 409–428.
- 1158 Holbrook, N. J., Scannell, H. A., Sen Gupta, A., Benthuisen, J. A., Feng, M.,
 1159 Oliver, E. C., ... Wernberg, T. (2019). A global assessment of marine
 1160 heatwaves and their drivers. *Nature Communications*, 10(1), 1–13. doi:
 1161 10.1038/s41467-019-10206-z
- 1162 Holbrook, N. J., Sen Gupta, A., Oliver, E. C. J., Hobday, A. J., Benthuisen,
 1163 J. A., Scannell, H. A., ... Wernberg, T. (2020). Keeping pace with ma-
 1164 rine heatwaves. *Nature Reviews Earth & Environment*, 1(9), 482–493. doi:
 1165 10.1038/s43017-020-0068-4
- 1166 Hunke, E., & Lipscomb, W. (2008). *CICE: The Los Alamos sea ice model documen-
 1167 tation and software user's manual version 4.0* (Tech. Rep.). Los Alamos NM
 1168 87545: T-3 Fluid Dynamics Group, Los Alamos National Laboratory.
- 1169 Jacox, M. G. (2019). Marine heatwaves in a changing climate. *Nature*, 571(7766),
 1170 485–487. doi: 10.1038/d41586-019-02196-1
- 1171 Johnson, K., & Claustre, H. (2016). The scientific rationale, design, and implemen-
 1172 tation plan for a Biogeochemical-Argo float array. *Biogeochemical-Argo Plan-
 1173 ning Group*. doi: 10.13155/46601
- 1174 Jorda, G., Marbà, N., Bennett, S., Santana-Garcon, J., Agusti, S., & Duarte,
 1175 C. M. (2020). Ocean warming compresses the three-dimensional habi-
 1176 tat of marine life. *Nature Ecology and Evolution*, 4(1), 109–114. doi:
 1177 10.1038/s41559-019-1058-0
- 1178 José, Y. S., Stramma, L., Schmidtko, S., & Oschlies, A. (2019). ENSO-driven fluc-
 1179 tuations in oxygen supply and vertical extent of oxygen-poor waters in the
 1180 oxygen minimum zone of the Eastern Tropical South Pacific. *Biogeosciences
 1181 Discussions*, 1–20.
- 1182 Kroeker, K. J., Kordas, R. L., Crim, R., Hendriks, I. E., Ramajo, L., Singh, G. S.,
 1183 ... Gattuso, J. P. (2013). Impacts of ocean acidification on marine organisms:
 1184 Quantifying sensitivities and interaction with warming. *Global Change Biology*,
 1185 19(6), 1884–1896. doi: 10.1111/gcb.12179

- 1186 Kwiatkowski, L., & Orr, J. C. (2018). Diverging seasonal extremes for ocean acidifi-
 1187 cation during the twenty-first century. *Nature Climate Change*, 8(2), 141–145.
 1188 doi: 10.1038/s41558-017-0054-0
- 1189 Kwiatkowski, L., Torres, O., Bopp, L., Aumont, O., Chamberlain, M., Christian,
 1190 J. R., . . . Ziehn, T. (2020). Twenty-first century ocean warming, acidifica-
 1191 tion, deoxygenation, and upper-ocean nutrient and primary production decline
 1192 from CMIP6 model projections. *Biogeosciences*, 17(13), 3439–3470. doi:
 1193 10.5194/bg-17-3439-2020
- 1194 Köhn, E. E., Münnich, M., Vogt, M., Desmet, F., & Gruber, N. (2022). Strong
 1195 Habitat Compression by Extreme Shoaling Events of Hypoxic Waters in the
 1196 Eastern Pacific. *Journal of Geophysical Research: Oceans*, 127(6). doi:
 1197 10.1029/2022jc018429
- 1198 Köhn, E. E., Vogt, M., Münnich, M., & Gruber, N. (2023). *On the vertical*
 1199 *structure and propagation of marine heatwaves in the Eastern Pacific.* doi:
 1200 10.22541/essoar.168565400.06607545/v1
- 1201 Lattuca, M. E., Vanella, F. A., Malanga, G., Rubel, M. D., Manríquez, P. H.,
 1202 Torres, R., . . . Fernández, D. A. (2023). Ocean acidification and sea-
 1203 sonal temperature extremes combine to impair the thermal physiology
 1204 of a sub-Antarctic fish. *Science of the Total Environment*, 856. doi:
 1205 10.1016/j.scitotenv.2022.159284
- 1206 Ledwell, J. R., St. Laurent, L. C., Girton, J. B., & Toole, J. M. (2011). Diapycnal
 1207 mixing in the antarctic circumpolar current. *Journal of Physical Oceanography*,
 1208 41(1), 241–246. doi: 10.1175/2010JPO4557.1
- 1209 Le Grix, N., Zscheischler, J., Laufkötter, C., Rousseaux, C. S., & Frölicher, T. L.
 1210 (2021). Compound high-temperature and low-chlorophyll extremes in the
 1211 ocean over the satellite period. *Biogeosciences*, 18(6), 2119–2137. doi:
 1212 10.5194/bg-18-2119-2021
- 1213 Le Grix, N., Zscheischler, J., Rodgers, K. B., Yamaguchi, R., & Frölicher, T. L.
 1214 (2022). Hotspots and drivers of compound marine heatwaves and low net
 1215 primary production extremes. *Biogeosciences*, 19(24), 5807–5835. doi:
 1216 10.5194/bg-19-5807-2022
- 1217 Leung, S., Mislán, K. A. S., Muhling, B., & Brill, R. (2019). The significance of
 1218 ocean deoxygenation for open ocean tunas and billfishes. In *Laffoley, D.*
 1219 *& Baxter, J.M. (eds.) (2019). Ocean deoxygenation: Everyone’s problem -*
 1220 *Causes, impacts, consequences and solutions.* (pp. 277–308). IUCN, Gland,
 1221 Switzerland. doi: 10.2305/IUCN.CH.2019.13.en
- 1222 Leung, S., Thompson, L. A., McPhaden, M. J., & Mislán, K. A. (2019). ENSO
 1223 drives near-surface oxygen and vertical habitat variability in the tropical Pa-
 1224 cific. *Environmental Research Letters*, 14(6). doi: 10.1088/1748-9326/ab1c13
- 1225 Luo, J. J., Zhang, R., Behera, S. K., Masumoto, Y., Jin, F. F., Lukas, R., & Ya-
 1226 magata, T. (2010). Interaction between El Niño and extreme Indian Ocean
 1227 dipole. *Journal of Climate*, 23(3), 726–742. doi: 10.1175/2009JCLI3104.1
- 1228 Luyten, R., J., Pedlosky, J., & Stommel, J. (1983). The Ventilated Thermocline.
 1229 *Journal of Physical Oceanography*. doi: 10.1175/1520-0485(1983)013<0292:
 1230 TVT>2.0.CO;2
- 1231 Ma, D., Gregor, L., & Gruber, N. (2023). Four Decades of Trends and Drivers
 1232 of Global Surface Ocean Acidification. *Global Biogeochemical Cycles*, 37(7),
 1233 e2023GB007765. doi: 10.1029/2023GB007765
- 1234 MacQueen, J. (1967). Some methods for classification and analysis of multivariate
 1235 observations. In *Proceedings of the fifth Berkeley symposium on mathematical*
 1236 *statistics and probability* (Vol. 1, pp. 281–297). Oakland, CA, USA.
- 1237 Marin, M., Feng, M., Bindoff, N. L., & Phillips, H. E. (2022). Local Drivers of
 1238 Extreme Upper Ocean Marine Heatwaves Assessed Using a Global Ocean
 1239 Circulation Model. *Frontiers in Climate*, 4. doi: 10.3389/fclim.2022.788390
- 1240 Masson-Delmotte, V., P. Z., A. Pirani, S. L. Connors, C. Péan, S. Berger, . . . B.

- 1241 Zhou (eds.) (2021). *IPCC, 2021: Summary for Policymakers. In: Climate*
 1242 *Change 2021: The Physical Science Basis. Contribution of Working Group*
 1243 *I to the Sixth Assessment Report of the Intergovernmental Panel on Climate*
 1244 *Change* (Tech. Rep.).
- 1245 Maulida, T., Wirasatriya, A., Ismunarti, D. H., & Puryajati, A. D. (2022). Physi-
 1246 cal drivers of the 2013 marine heatwave in the seas of the southern Java-Nusa
 1247 Tenggara. *Geographia Technica*, *17*, 129–139. doi: 10.21163/GT.2022.171.10
- 1248 McAdam, R., Masina, S., & Gualdi, S. (2022). Seasonal forecasting of subsurface
 1249 marine heat waves. *Submitted to Nature Communications*(2023), 1–11. doi: 10
 1250 .1038/s43247-023-00892-5
- 1251 Moore, J. K., Doney, S. C., & Lindsay, K. (2004). Upper ocean ecosystem dynam-
 1252 ics and iron cycling in a global three-dimensional model. *Global Biogeochemical*
 1253 *Cycles*, *18*(4), 1–21. doi: 10.1029/2004GB002220
- 1254 Moore, J. K., Lindsay, K., Doney, S. C., Long, M. C., & Misumi, K. (2013). Marine
 1255 ecosystem dynamics and biogeochemical cycling in the community earth sys-
 1256 tem model [CESM1(BGC)]: Comparison of the 1990s with the 2090s under the
 1257 RCP4.5 and RCP8.5 scenarios. *Journal of Climate*, *26*(23), 9291–9312. doi:
 1258 10.1175/JCLI-D-12-00566.1
- 1259 Morrison, A. K., Frölicher, T. L., & Sarmiento, J. L. (2015). Upwelling in the South-
 1260 ern Ocean. *Physics Today*, *68*(1), 27–32. doi: 10.1063/PT.3.2654
- 1261 Nam, S., Kim, H. J., & Send, U. (2011). Amplification of hypoxic and acidic events
 1262 by la Niña conditions on the continental shelf off California. *Geophysical Re-*
 1263 *search Letters*, *38*(22), 1–5. doi: 10.1029/2011GL049549
- 1264 Negrete-García, G., Lovenduski, N. S., Hauri, C., Krumhardt, K. M., & Lauvset,
 1265 S. K. (2019). Sudden emergence of a shallow aragonite saturation hori-
 1266 zon in the Southern Ocean. *Nature Climate Change*, *9*(4), 313–317. doi:
 1267 10.1038/s41558-019-0418-8
- 1268 Oliver, E. C., Benthuyzen, J. A., Darmaraki, S., Donat, M. G., Hobday, A. J., Hol-
 1269 brook, N. J., ... Gupta, A. S. (2021). Marine Heatwaves. *Annual Review of*
 1270 *Marine Science*, *13*(1), 1–30. doi: 10.1146/annurev-marine-032720-095144
- 1271 Oliver, E. C., Donat, M. G., Burrows, M. T., Moore, P. J., Smale, D. A., Alexan-
 1272 der, L. V., ... Wernberg, T. (2018). Longer and more frequent marine
 1273 heatwaves over the past century. *Nature Communications*, *9*(1), 1–12. doi:
 1274 10.1038/s41467-018-03732-9
- 1275 Orr, J. C., Fabry, V. J., Aumont, O., Bopp, L., Doney, S. C., Feely, R. A., ... Yool,
 1276 A. (2005). Anthropogenic ocean acidification over the twenty-first cen-
 1277 tury and its impact on calcifying organisms. *Nature*, *437*, 681–686. doi:
 1278 10.1038/nature04095
- 1279 Pan, T. C., Applebaum, S. L., & Manahan, D. T. (2015). Experimental ocean acid-
 1280 ification alters the allocation of metabolic energy. *Proceedings of the National*
 1281 *Academy of Sciences of the United States of America*, *112*(15), 4696–4701. doi:
 1282 10.1073/pnas.1416967112
- 1283 Paulmier, A., & Ruiz-Pino, D. (2009). Oxygen minimum zones (OMZs) in
 1284 the modern ocean. *Progress in Oceanography*, *80*(3-4), 113–128. Re-
 1285 trieved from <http://dx.doi.org/10.1016/j.pocean.2008.08.001> doi:
 1286 10.1016/j.pocean.2008.08.001
- 1287 Paulmier, A., Ruiz-Pino, D., & Garçon, V. (2011). CO₂ maximum in the oxygen
 1288 minimum zone (OMZ). *Biogeosciences*, *8*(2), 239–252. doi: 10.5194/bg-8-239
 1289 -2011
- 1290 Pellichero, V., Sallée, J.-B., Schmidtko, S., Roquet, F., & Charrassin, J.-B. (2017).
 1291 The ocean mixed layer under Southern Ocean sea-ice: Seasonal cycle and
 1292 forcing. *Journal of Geophysical Research: Oceans*, *122*(2), 1608–1633. doi:
 1293 10.1002/2016JC011970
- 1294 Pirotta, E., Thomas, L., Costa, D. P., Hall, A. J., Harris, C. M., Harwood, J., ...
 1295 Tyack, P. L. (2022). Understanding the combined effects of multiple stres-

- 1296 sors: A new perspective on a longstanding challenge. *Science of the Total*
 1297 *Environment*, 821, 153322. doi: 10.1016/j.scitotenv.2022.153322
- 1298 Pörtner, H. O. (2002). Climate variations and the physiological basis of temperature
 1299 dependent biogeography: Systemic to molecular hierarchy of thermal toler-
 1300 ance in animals. *Comparative Biochemistry and Physiology - A Molecular and*
 1301 *Integrative Physiology*, 132(4), 739–761. doi: 10.1016/S1095-6433(02)00045-4
- 1302 Pörtner, H. O., & Knust, R. (2007). Climate Change Affects Marine Fishes Through
 1303 the Oxygen Limitation of Thermal Tolerance. *Science*, 315, 95–97. doi: 10
 1304 .1259/0007-1285-53-633-920-b
- 1305 Qi, R., Zhang, Y., Du, Y., & Feng, M. (2022). Characteristics and Drivers of Ma-
 1306 rine Heatwaves in the Western Equatorial Indian Ocean. *Journal of Geophysi-
 1307 cal Research: Oceans*, 127(10), e2022JC018732. doi: 10.1029/2022JC018732
- 1308 Ramadhan, A., Marshall, J., Meneghello, G., Illari, L., & Speer, K. (2022). Obser-
 1309 vations of Upwelling and Downwelling Around Antarctica Mediated by Sea Ice.
 1310 *Frontiers in Marine Science*, 9. doi: 10.3389/fmars.2022.864808
- 1311 Righetti, D., Vogt, M., Gruber, N., Psomas, A., & Zimmermann, N. E. (2019).
 1312 Global pattern of phytoplankton diversity driven by temperature and environ-
 1313 mental variability. *Science Advances*, 5(5). doi: 10.1126/sciadv.aau6253
- 1314 Riquelme-Bugueño, R., Pérez-Santos, I., Alegría, N., Vargas, C. A., Urbina, M. A.,
 1315 & Escribano, R. (2020). Diel vertical migration into anoxic and high-pCO₂
 1316 waters: acoustic and net-based krill observations in the Humboldt Current.
 1317 *Scientific Reports*, 10(1), 1–11. doi: 10.1038/s41598-020-73702-z
- 1318 Ritz, D. A., Hobday, A. J., Montgomery, J. C., & Ward, A. J. W. (2011). Chapter
 1319 Four - Social Aggregation in the Pelagic Zone with Special Reference to Fish
 1320 and Invertebrates. In M. Lesser (Ed.), *Advances in Marine Biology* (Vol. 60,
 1321 pp. 161–227). Academic Press. doi: 10.1016/B978-0-12-385529-9.00004-4
- 1322 Rose, K., Gutiérrez, D., Breitburg, D., Conley, D., Craig, K., Froehlich, H., ...
 1323 Prema, D. (2019). Impacts of ocean deoxygenation on fisheries. In *Laffoley,*
 1324 *D. & Baxter, J.M. (eds.) (2019). Ocean deoxygenation: Everyone's problem*
 1325 *- Causes, impacts, consequences and solutions.* (pp. 519–544). IUCN, Gland,
 1326 Switzerland. doi: 10.2305/IUCN.CH.2019.13.en
- 1327 Rosselló, P., Pascual, A., & Combes, V. (2023). Assessing marine heat waves in the
 1328 Mediterranean Sea: a comparison of fixed and moving baseline methods. *Fron-*
 1329 *tiers in Marine Science*, 10, 1168368. doi: 10.3389/fmars.2023.1168368
- 1330 Roy, C., & Reason, C. (2001). ENSO related modulation of coastal upwelling in the
 1331 eastern Atlantic. *Progress in Oceanography*, 49(1-4), 245–255. doi: 10.1016/
 1332 S0079-6611(01)00025-8
- 1333 Samuels, T., Rynearson, T. A., & Collins, S. (2021). Surviving Heatwaves: Thermal
 1334 Experience Predicts Life and Death in a Southern Ocean Diatom. *Frontiers in*
 1335 *Marine Science*, 8. doi: 10.3389/fmars.2021.600343
- 1336 Santoso, A., Mcphaden, M. J., & Cai, W. (2017). The Defining Characteristics
 1337 of ENSO Extremes and the Strong 2015/2016 El Niño. *Reviews of Geophysics*,
 1338 55(4), 1079–1129. doi: 10.1002/2017RG000560
- 1339 Scannell, H. A., Johnson, G. C., Thompson, L., Lyman, J. M., & Riser, S. C.
 1340 (2020). Subsurface Evolution and Persistence of Marine Heatwaves in
 1341 the Northeast Pacific. *Geophysical Research Letters*, 47(23), 1–10. doi:
 1342 10.1029/2020GL090548
- 1343 Schaeffer, A., & Roughan, M. (2017). Subsurface intensification of marine heatwaves
 1344 off southeastern Australia: The role of stratification and local winds. *Geophysi-
 1345 cal Research Letters*, 44(10), 5025–5033. doi: 10.1002/2017GL073714
- 1346 Seibel, B. A. (2011). Critical oxygen levels and metabolic suppression in oceanic
 1347 oxygen minimum zones. *Journal of Experimental Biology*, 214(2), 326–336.
 1348 doi: 10.1242/jeb.049171
- 1349 Seibel, B. A., Schneider, J. L., Kaartvedt, S., Wishner, K. F., & Daly, K. L.
 1350 (2016). Hypoxia Tolerance and Metabolic Suppression in Oxygen Mini-

- 1351 mum Zone Euphausiids: Implications for Ocean Deoxygenation and Biogeo-
 1352 chemical Cycles. *Integrative and Comparative Biology*, 56(4), 510–523. doi:
 1353 10.1093/icb/icw091
- 1354 Sen Gupta, A. (2023). *Marine heatwaves: definition duel heats up*.
- 1355 Sen Gupta, A., Thomsen, M., Benthuisen, J. A., Hobday, A. J., Oliver, E., Alexan-
 1356 der, L. V., . . . Smale, D. A. (2020). Drivers and impacts of the most
 1357 extreme marine heatwaves events. *Scientific Reports*, 10(1), 1–15. doi:
 1358 10.1038/s41598-020-75445-3
- 1359 Smale, D. A., Wernberg, T., Oliver, E. C. J., Thomsen, M., Harvey, B. P., Straub,
 1360 S. C., . . . Moore, P. J. (2019). Marine heatwaves threaten global biodiversi-
 1361 ty and the provision of ecosystem services. *Nature Climate Change*, 9(4),
 1362 306–312. doi: 10.1038/s41558-019-0412-1
- 1363 Smith, K. E., Burrows, M. T., Hobday, A. J., King, N. G., Moore, P. J., Sen Gupta,
 1364 A., . . . Smale, D. A. (2023). Biological Impacts of Marine Heatwaves. *Annual*
 1365 *review of marine science*, 15, 119–145. doi: 10.1146/annurev-marine-032122-
 1366 -121437
- 1367 Smith, R., & Gent, P. (2010). *The Parallel Ocean Program (POP) reference manual*
 1368 (Tech. Rep.). National Center for Atmospheric Research Boulder, Colorado:
 1369 National Center for Atmospheric Research Boulder, Colorado.
- 1370 Stabeno, P. J., & Bell, S. W. (2019). Extreme Conditions in the Bering Sea
 1371 (2017–2018): Record-Breaking Low Sea-Ice Extent. *Geophysical Research*
 1372 *Letters*, 46(15), 8952–8959. doi: 10.1029/2019GL083816
- 1373 Stuart-Smith, R. D., Bates, A. E., Lefcheck, J. S., Duffy, J. E., Baker, S. C., Thom-
 1374 son, R. J., . . . Edgar, G. J. (2013). Integrating abundance and functional
 1375 traits reveals new global hotspots of fish diversity. *Nature*, 501(7468), 539–542.
 1376 doi: 10.1038/nature12529
- 1377 Susanto, R. D., Gordon, A. L., & Zheng, Q. (2001). Upwelling along the coasts
 1378 of Java and Sumatra and its relation to ENSO. *Geophysical Research Letters*,
 1379 28(8), 1599–1602. doi: 10.1029/2000GL011844
- 1380 Tai, T. C., Sumaila, U. R., & Cheung, W. W. (2021). Ocean Acidification Ampli-
 1381 fies Multi-Stressor Impacts on Global Marine Invertebrate Fisheries. *Frontiers*
 1382 *in Marine Science*, 8, 1–12. doi: 10.3389/fmars.2021.596644
- 1383 Tamsitt, V., Drake, H. F., Morrison, A. K., Talley, L. D., Dufour, C. O., Gray,
 1384 A. R., . . . Weijer, W. (2017). Spiraling pathways of global deep waters to
 1385 the surface of the Southern Ocean. *Nature Communications*, 8(1), 1–10. doi:
 1386 10.1038/s41467-017-00197-0
- 1387 Turi, G., Alexander, M., Lovenduski, N. S., Capotondi, A., Scott, J., Stock, C., . . .
 1388 Jacox, M. (2018). Response of O₂ and pH to ENSO in the California Current
 1389 System in a high-resolution global climate model. *Ocean Science*, 14(1), 69–86.
 1390 doi: 10.5194/os-14-69-2018
- 1391 Vogt, L., Burger, F. A., Griffies, S. M., & Frölicher, T. L. (2022). Local Drivers of
 1392 Marine Heatwaves: A Global Analysis With an Earth System Model. *Frontiers*
 1393 *in Climate*, 4. doi: 10.3389/fclim.2022.847995
- 1394 Wilson, E. A., Riser, S. C., Campbell, E. C., & Wong, A. P. (2019). Winter
 1395 upper-ocean stability and ice-ocean feedbacks in the sea ice-covered South-
 1396 ern Ocean. *Journal of Physical Oceanography*, 49(4), 1099–1117. doi:
 1397 10.1175/JPO-D-18-0184.1
- 1398 Worm, B., & Tittensor, D. P. (2018). *A theory of global biodiversity* (No. 60).
 1399 Princeton, New Jersey: Princeton University Press.
- 1400 Xu, K., Huang, R. X., Wang, W., Zhu, C., & Lu, R. (2017). Thermocline fluctua-
 1401 tions in the equatorial pacific related to the two types of El Niño events. *Jour-*
 1402 *nal of Climate*, 30(17), 6611–6627. doi: 10.1175/JCLI-D-16-0291.1
- 1403 Yang, G., Liu, L., Zhao, X., Li, Y., Duan, Y., Liu, B., . . . Yu, W. (2019). Impacts
 1404 of Different Types of ENSO Events on Thermocline Variability in the Southern
 1405 Tropical Indian Ocean. *Geophysical Research Letters*, 46(12), 6775–6785. doi:

- 1406 10.1029/2019GL082818
1407 Yang, S., & Gruber, N. (2016). The anthropogenic perturbation of the marine ni-
1408 trogen cycle by atmospheric deposition: Nitrogen cycle feedbacks and the 15N
1409 Haber-Bosch effect. *Global Biogeochemical Cycles*, *30*(10), 1418–1440. doi:
1410 10.1002/2016GB005421
- 1411 Zeebe, R. E., & Wolf-Gladrow, D. (2001). *CO₂ in seawater : equilibrium, kinetics,*
1412 *isotopes*. Burlington: Elsevier Burlington.
- 1413 Zhang, Y., Du, Y., Feng, M., & Hu, S. (2021). Long-Lasting Marine Heat-
1414 waves Instigated by Ocean Planetary Waves in the Tropical Indian Ocean
1415 During 2015–2016 and 2019–2020. *Geophysical Research Letters*, *48*(21),
1416 e2021GL095350. doi: 10.1029/2021GL095350
- 1417 Zscheischler, J., & Seneviratne, S. I. (2017). Dependence of drivers affects risks as-
1418 sociated with compound events. *Science Advances*, *3*(6), 1–11. doi: 10.1126/
1419 sciadv.1700263
- 1420 Zuo, H., Balmaseda, M. A., Tietsche, S., Mogensen, K., & Mayer, M. (2019). The
1421 ECMWF operational ensemble reanalysis–analysis system for ocean and sea
1422 ice: a description of the system and assessment. *Ocean Science*, *15*(3), 779–
1423 808. doi: 10.5194/os-15-779-2019